Acta Astronautica 147 (2018) 316–345

Contents lists available at ScienceDirect

Acta Astronautica

journal homepage: www.elsevier.com/locate/actaastro

A comprehensive assessment of collision likelihood in Geosynchronous Earth Orbit

D.L. Oltrogge[a,*], S. Alfano[a], C. Law[b], A. Cacioni[c], T.S. Kelso[d]

[a] Centre for Space Standards and Innovation, Analytical Graphics Inc., 7150 Campus Drive, Suite 260, Colorado Springs, CO, 80920, United States
[b] Flight Dynamics, SES, Chateau de Betzdorf, Luxembourg
[c] Flight Dynamics, Inmarsat, 99 City Road, London, Greater London, EC1Y1AX, United Kingdom
[d] Center for Space Standards and Innovation (CSSI), 7150 Campus Drive, Suite 260, Colorado Springs, CO, 80920-6522, United States

ARTICLE INFO

Keywords:
GEO collision likelihood
Encounter rate
Comprehensive
Collision risk

ABSTRACT

Knowing the likelihood of collision for satellites operating in Geosynchronous Earth Orbit (GEO) is of extreme importance and interest to the global community and the operators of GEO spacecraft. Yet for all of its importance, a comprehensive assessment of GEO collision likelihood is difficult to do and has never been done. In this paper, we employ six independent and diverse assessment methods to estimate GEO collision likelihood. Taken in aggregate, this comprehensive assessment offer new insights into GEO collision likelihood that are within a factor of 3.5 of each other. These results are then compared to four collision and seven encounter rate estimates previously published. Collectively, these new findings indicate that collision likelihood in GEO is as much as four orders of magnitude higher than previously published by other researchers. Results indicate that a collision is likely to occur every 4 years for one satellite out of the entire GEO active satellite population against a 1 cm RSO catalogue, and every 50 years against a 20 cm RSO catalogue. Further, previous assertions that collision relative velocities are low (i.e., < 1 km/s) in GEO are disproven, with some GEO relative velocities as high as 4 km/s identified. These new findings indicate that unless operators successfully mitigate this collision risk, the GEO orbital arc is and will remain at high risk of collision, with the potential for serious follow-on collision threats from post-collision debris when a substantial GEO collision occurs.

1. Introduction

Knowing the likelihood of collision for satellites is of extreme importance and interest to the global space community, satellite operators and the space insurance industry alike. This is especially true in GEO due to both the high cost to build, launch and operate GEO satellites, the importance of maintaining the safety and commercial viability of the GEO orbit regime, and the continual noncompliance by some GEO operators with existing space debris mitigation guidelines, best practices and expected norms of behaviour [1]. Yet for all of its importance, a comprehensive assessment of the likelihood of GEO collisions has not been accomplished to date. This is likely due to the complexities involved:

(1) The synchronous nature of satellites in GEO, which presents problems for typical approaches to assessing the likelihood of a collision;
(2) orbit perturbations in GEO (primarily gravity wells, soli-lunar perturbations and Solar Radiation Pressure) that cause satellite orbits to move out of the equatorial plane (north/south) as well as to drift in a longitudinally-dependent east/west cycle;
(3) unknown/unpredictable operator operations and collision avoidance strategies; and
(4) the lack of methods available to estimate long-term encounter rates independent of our Space Situational Awareness knowledge.

NASA became concerned about GEO crowding in 1980 [2]. The distribution of active satellites in the GEO belt is far from uniform, with a greater concentration over the continents than the oceans. Objects drifting through the GEO belt have a greater concentration about the gravity wells at 105° W and 75° E. Although our figures show variability of satellite locations and threatening objects, the individual threat to each and every GEO satellite is beyond the scope of this paper.

Rather, we wish to capture the collective threat to the entire GEO belt. Such an approach allows us to compare and contrast the various approaches of others in a common framework. As will be explained for

* Corresponding author.
E-mail addresses: oltrogge@agi.com (D.L. Oltrogge), salfano@agi.com (S. Alfano), Charles.law@ses.com (C. Law), alex.cacioni@inmarsat.com (A. Cacioni), tskelso@agi.com (T.S. Kelso).

https://doi.org/10.1016/j.actaastro.2018.03.017
Received 24 October 2017; Received in revised form 6 March 2018; Accepted 10 March 2018
Available online 12 March 2018

Nomenclature

a	semi-major axis
e	orbit eccentricity
η	angle between relative velocity vector and GEO primary's long axis (≈inertial Z axis direction)
i	orbit inclination
J_2	zonal gravity coefficient = $-C_{2,0}$
$\mathcal{L}_{YYY}$	Collision likelihood for conditions YYY
MA1	mean anomaly of satellite one (secondary)
MA2	mean anomaly of satellite two (primary)
M	molar mass
m	molecular mass
ν	orbit true anomaly
n	number of moles
N	number of molecules = n N_A
N_A	Avogadro's number = 6.0221 × 1023/mol
N_V	number of molecules per unit volume = $\frac{n\,N_A}{V}$
Ω	Right Ascension of Ascending Node (RAAN)
Ω_E	Encounter angle between relative velocity ($\overline{v}_{secondary} - \overline{v}_{primary}$) and $\overline{v}_{primary}$
ω	argument of perigee
P	absolute pressure
p	semi-latus rectum
R	universal gas constant = 8.3145 J/mol K
R_E	attracting body's equatorial radius
R_{ENC}	encounter (screening threshold) radius
$SF_{OffN/S}$	scale factor to convert cross-track-derived encounter rates to observed encounter angles
SF_{T2C}	scale factor of tracked to correlated RSOs
$SF_{T2C\ active}$	scale factor of tracked to correlated RSOs
$SF_{T2C\ inactive}$	scale factor of tracked to correlated RSOs
T	absolute temperature
$\overline{\Delta t}_{mc}$	average time between molecular collisions
V	volume

Acronyms/Abbreviations

ACP	Annual Collision Probability
AdvCAT	Advanced Conjunction Assessment Tool
AGI	Analytical Graphics Inc.
CDM	Conjunction Data Message
CSSI	Center for Space Standards and Innovation
DREAD	Debris Risk Evolution and Dispersal
ESA	European Space Agency
FDS	Flight Dynamics Staff
GEO	Geosynchronous Earth Orbit
GTO	Geosynchronous Transfer Orbit
HEO	Highly Elliptical Orbit
JSpOC	Joint Space Operations Center
KGT	Kinetic Gas Theory
LEO	Low Earth Orbit
MEO	Medium Earth Orbit
PDF	Probability Density Function
RSO	Resident Space Object
SATCAT	Satellite Catalogue
SDA	Space Data Association
STK	Systems Tool Kit
TCA	Time of Closest Approach
USSTRAT COM	United States Strategic Command

each method, we do this by taking those results and adjusting them to assess the entire threat to the largest GEO satellite operators participating in the Space Data Association (the "SDA Big 4") who in 2014 collectively operated 167 GEO satellites.

Over the three-year study period of this paper, that number of active satellites has changed very little; at present (2017), they operate 168 satellites. For the purposes of this study, a fixed number of 167 will be adopted for the rest of this paper. We'll then use that estimated likelihood of a collision for this set of 167 satellites to estimate collision likelihood for the entire GEO active satellite population.

New methods for determining typical encounter rates for extant spacecraft sizes, coupled with statistics gleaned from diverse and comprehensive conjunction alert datasets, offer ways to address these technical complexities. In this paper, we employ many of these new methods to estimate the likelihood of a GEO collision and compare the results between our methods. Taken in aggregate, these methods offer new insights into the likelihood of GEO collision that are in large part consistent with each other to within one order of magnitude. These results are then compared to any/all relevant estimates and encounter rate assessments done by independent researchers. The new results indicate that the likelihood of a GEO collision appears to be as much as four orders of magnitude higher than had previously been estimated by some researchers.

2. The current public space population

Since 1957, the US Space Surveillance Network has been detecting, tracking, cataloguing, and identifying artificial objects orbiting Earth. In their public catalogue [3], these objects include both active (9.6%) and inactive (14.6%) satellites, spent rocket bodies (11.5%), and fragmentation debris (64.3%) [4]. The 26 Aug 2017 public space catalogue maintained by the JSpOC contains 1366 RSOs which traverse this same GEO ± 100 km altitude range, of which 888 are inactive and 478 are active as defined by the SATCAT on CelesTrak [5].

2.1. Identified sources of debris in GEO

Sources of debris smaller than 1 m in size typically include: disintegration, erosion, collisions, detachment of coatings and paint flakes, accidental or intentional mission release, accidental fragmentation such as fuel tank explosions, intentional fragmentation from anti-satellite vehicle testing, and particles released by solid rocket motors firings as well as leaked coolant. Observations of the current GEO space population indicate that a number of GEO fragmentation events have already occurred. Accompanying the data shown in Fig. 1, Flegel [6] states, "*only two fragmentation events have been officially confirmed to have occurred in geosynchronous orbits (Johnson* et al. *2008). Oswald* et al.

Table 8.1: List of GEO fragmentation events from MASTER-2009. Table is reproduced from Flegel et al. (2011c)

Event Type	Int. Desig.	Name	m / kg	Epoch / yyddd.d	a / km	i / °
Known	1977-092A	Ekran-2	1970	78174.0	42182.3	0.1
Known	1968-081E	Titan 3C Transtage 5	1950	92053.4	41835.4	11.9
Unconfirmed	1973-040B	Titan 3C Transtage 24	1950	81067.2	42345.7	5.9
Unconfirmed	1979-087A	Ekran-4	1970	82157.8	42158.1	1.7
Unconfirmed	1979-053C	Titan 3C Transtage 30	1950	82309.0	42403.8	0.6
Unconfirmed	1975-118C	Titan 3C Transtage 28	1950	87072.6	42101.8	8.6
Unconfirmed	1966-053J	Titan 3C Transtage 11	1950	87276.7	40497.2	11.5
Unconfirmed	1967-066G	Titan 3C Transtage 14	1950	94045.4	39842.9	11.7
Unconfirmed	1975-117A	SatCom 1	463	99257.7	42354.6	12.0
Unconfirmed	1988-018B	Telecom 1C	1210	02263.0	42826.4	5.8
Artificial	-	Artificial 1	1750	98180.0	40164.0	0.3
Artificial	-	Artificial 2	1750	92280.0	44850.0	2.0

Fig. 1. Known & unconfirmed GEO fragmentations [6] (used by permission of author).

(2006) lists a total of 21 additional suspected GEO anomalies from which eight were introduced into the MASTER-2009 population as fragmentations." Krag et al. [7] concluded that "*The GEO and GTO surveys of the ESA Space Debris Telescope revealed a considerable population of objects that cannot only be explained by so-far unknown fragmentation events. ESA's MASTER model had to be adjusted by the introduction of additional fragmentation events on GEO and by an enhancement of the number of objects released during GTO fragmentations. … Objects on Molniya orbits have the potential to interfere with the GEO protected region."*

2.2. Estimated space population in GEO

The US Space Surveillance Network (SSN) catalogue nominally includes objects larger than 1 m in geosynchronous orbit (GEO – 24-h orbit) [8]. The resulting lack of situational awareness below 1 m object size is primarily due to the limited amount of debris tracking and survey data available to date, coupled with the lack of knowledge of fragmentation events mentioned above. Germane to this paper, this limitation presents a huge challenge to assessing the likelihood of a collision in that the debris environment in GEO is not well-understood, especially for debris fragment sizes that pose significant risk which can easily (a) disable a GEO satellite (perhaps 1–10 cm in size); and (b) generate additional large quantities of GEO debris fragments (perhaps > 20 cm).

The few GEO space population estimates we do have are derived from space debris surveys [9] as shown in Fig. 2. Such debris survey data has been incorporated into space population models such as NASA's ORDEM model and ESA's MASTER 2009 model [10].

Recent methods [11] allow the assembly of space catalogues consistent with current space population models and that are representative with what is believed to be orbiting the Earth down to arbitrarily-small size. These were employed to create the characterizations shown in Fig. 3 (GEO ± 100 km) and Fig. 4 (GEO-200km through GEO + 800 km). The breakdown of debris sizes in Fig. 3 is consistent with Krezan et al. [12], who estimated, based on NASA-WISE data, that there are between 1036–3060 debris fragments greater than 10 cm, and 35,458–157,956 fragments greater than 1 cm.

The aforementioned 1366 GEO objects comprise only 4% of the estimated 33,239 GEO-crossing objects larger than 1 cm (Fig. 3) [13,14]. Having only a four percent awareness of one's space situation is viewed by many as insufficient.

A consistency check of Fig. 4 results with Fig. 2 can readily be performed by ensuring that the ratio of "correlated" (or contained in the public RSO catalogue) blue bars to "uncorrelated" (or unrepresented in the public RSO catalogue dimmer than visual magnitude 15) red bars matches in the two estimates.

From ESA's debris survey (Fig. 2), adding up the digitized bars yields 314 correlated detection ("Frequency") occurrences (blue bars), 105 uncorrelated detection occurrences (red bars brighter than Vmag 15) and 297 untracked detection occurrences (red bars dimmer than ≈ Vmag 15). This yields a ratio of tracked-to-untracked detections of 419:297 or 1.41. Defining the scale factor of total (active and inactive) tracked objects to tracked and correlated objects as:

$$SF_{T2C\ active} = \left[\frac{\frac{478_{active}}{1366}314 + f_a 105}{\frac{478_{active}}{1366}314}\right] \tag{1}$$

where f_a is the (unknown) fraction of uncorrelated objects that are active. Parametric evaluation of f_a from 0.0 to 1.0 yields $1.0 < SF_{T2C\ active} < 1.96$ (median of 1.48).

$$SF_{T2C\ inactive} = \left[\frac{\frac{888_{inactive}}{1366}314 + (1 - f_a)105}{\frac{888_{inactive}}{1366}314}\right] \tag{2}$$

Parametric evaluation of f_a from 0.0 to 1.0 yields $1.52 < SF_{T2C} < 1.0$ (median of 1.26).

$$SF_{T2C} = SF_{T2C\ active} SF_{T2C\ inactive} \tag{3}$$

Parametric evaluation of f_a from 0.0 to 1.0 yields $1.52 < SF_{T2C} < 1.96$ (median of 1.86).

By comparison, when our estimates (Fig. 4) were created (2016), there were 1712 RSOs ≈ ≥ 1 m (GEO-200 to GEO + 800 km) in the public catalogue with 466 active. From Fig. 4, there are 3344 RSOs larger than 10 cm and (3344–1712) = 1626 estimated to be between 10 cm and 1 m. This yields an equivalent ratio of public-to-untracked detections of 1712: 1626 = 1.0529. This compares very favourably with the ratio of 1.0572 obtained from analysis of public-to-untracked detections in Fig. 2.

3. GEO S/C dimensions and orientation

When assessing collision likelihood, it is critical to properly incorporate the overall size, shape and attitude of the two space objects at the Time of Closest Approach (TCA). Satellites come in all shapes and sizes, and GEO satellites are no exception. A popular GEO satellite (which also is currently one of the largest) is the Boeing 702 bus shown in Fig. 5 [16], whose length is comparable to the wingspan of a 737 aircraft [17] as shown in Fig. 6.

The Boeing 702 bus is 42 m in length, and roughly 6–8 m in width and height, discounting the four extended parabolic dishes.

The likelihood of collision is directly proportional to the cross-sectional area presented by each satellite to the other one. As will soon be discussed, a GEO satellite's typical north/south alignment (Fig. 5 [16]) couples favourably with the typical relative motion approach angle (Fig. 7) to minimize the likelihood of a collision.

Figs. 8–10 contain to-scale orthogonal views of the Boeing 702 bus in its typical orientation on-orbit. For the purpose of this paper and based on the dimensions of this satellite as portrayed by Fig. 10, a "collision" with an assumed 2 m spherical debris object is defined to be a close approach within half of the Boeing 702's roughly 8 m cross-sectional dimension viewed north/south (i.e., radius of 4 m) plus half of the 2 m debris object's diameter, for a total allowable miss distance of 5 m. This 5 m number represents our assumed lower limit for combined hardbody object size for the remainder of this paper.

4. Characterization of GEO close approaches using JSpOC conjunction data message repository

While this paper is primarily focused on assessing the average likelihood that an active GEO satellite will generically "encounter" (or specifically collide with, if the encounter screening radius matches the combined hardbody radii of the conjuncting objects) another GEO satellite, an interesting by-product is that much can be gleaned from statistically characterizing the close approach data obtained from operational conjunction assessment systems. USSTRATCOM has

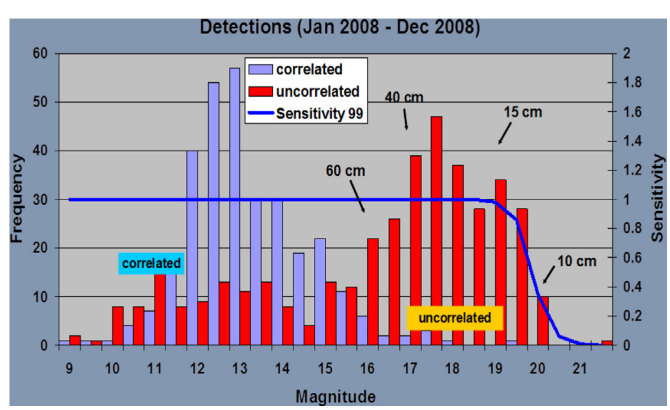

Fig. 2. GEO object detections obtained in ESA's optical sensor debris campaign (2008) [15] (included by permission of author).

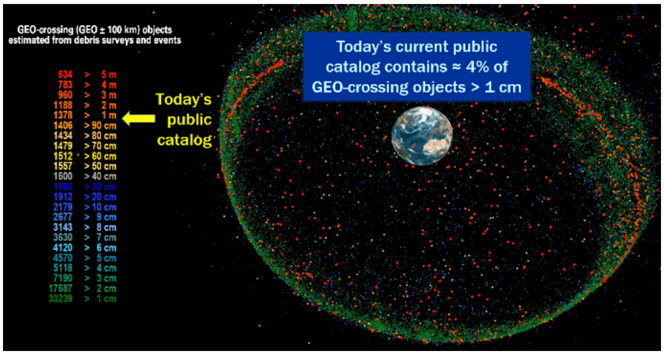

Fig. 3. Estimated GEO-crossing objects > 1 cm in GEO ± 100 km altitude vs the 2017 1366 RSO GEO-crossing public catalogue.

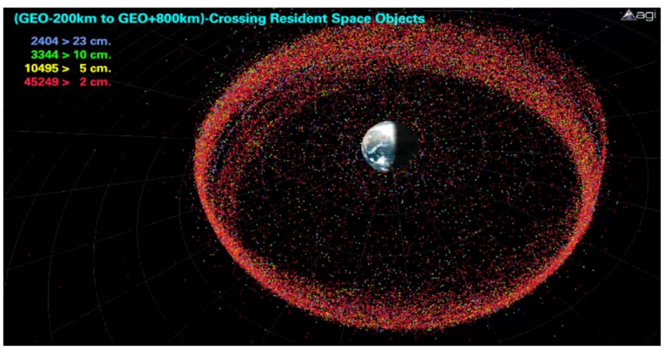

Fig. 4. Estimated GEO-crossing objects larger than 2 cm in GEO-200km through GEO + 800 km.

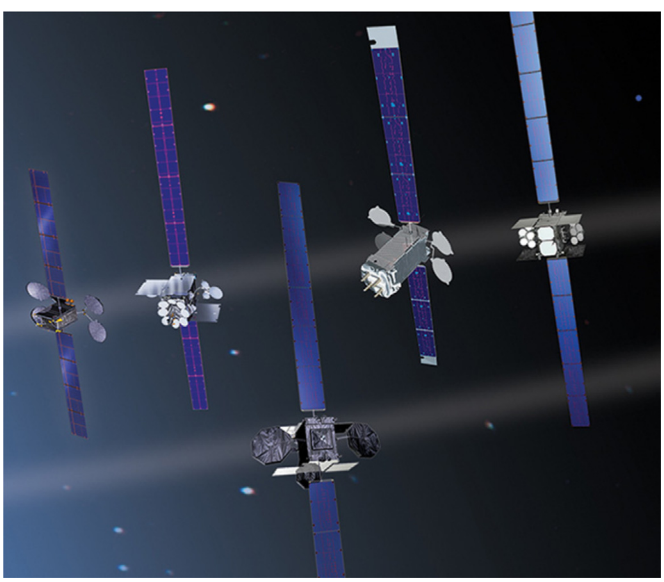

Fig. 5. Boeing 702 satellites flying in their typical GEO satellite orientation, with long dimension aligned north/south to allow the solar arrays to track Sun.

graciously authorized the authors to aggregate statistics from the Conjunction Data Messages (CDMs) received as part of Space Data Center operations and AGI's standing support to the 33 operators participating in the Space Data Association, 18 of which operate satellites in GEO.

For the period 25 April 2014 to 19 May 2017 (3.066393 years), CSSI received 975,735 CDMs for 26 satellite operators having signed SSA Data Sharing agreements in place with USSTRATCOM. Of those CDMs, 648,214 CDMs corresponded to unique Times of Closest Approach

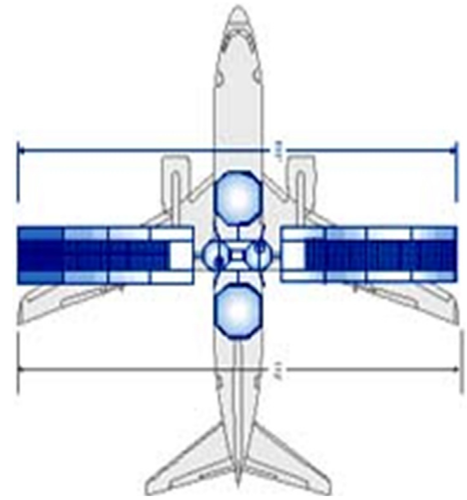

Fig. 6. Comparison of the 42 m "wingspans" of both the Boeing 737 aircraft and the Boeing 702 satellite.

(TCAs). Further confining the conjunctions to occur within ± 100 km of GEO altitude (i.e., a radius magnitude of 42,064–42,264 km) yielded 402,950 remaining conjunctions, with the largest miss distance at TCA of 363 km. We then discarded all "in-fleet" conjunctions (i.e., those conjunctions occurring within an operator's own fleet, because the operator presumably will ensure they do not hit themselves), leaving 353,161 conjunctions. These conjunctions will be used later to characterize the number of encounters as a function of miss distance using JSpOC data.

But for the following section, we want to characterize actual GEO collision risk conditions by further restricting miss distance to be less than 10 km at TCA (yielding 34,001 conjunctions).

4.1. Close conjunction statistics

As just discussed, GEO spacecraft can be extremely long in comparison to their other dimensions. But collision probability depends in large part upon the cross-sectional area that the primary satellite presents to the approaching collision threat object. Therefore it is imperative to understand the orientation of GEO spacecraft relative to approaching collision threats. In preparation for examining this, we define "encounter angle" Ω_E as shown in Fig. 11, where Ω_E is simply the angle between the relative velocity vector in inertial space and the primary's inertial velocity vector.

Using this encounter angle Ω_E definition, Fig. 12 and Fig. 13 show that while encounter angles can range anywhere from 0° to 180°, the preponderance of them (median value) is around 86°, contrasting with a median encounter angle of approximately 35° in LEO as shown in Ref. [20]. This indicates that "broadside" conjunctions (and collisions) are the most common mode in GEO, which is consistent with the satellite size discussion from the previous section and also makes sense given that the slightest "relative inclination" between the GEO active satellite and a conjuncting satellite or debris will introduce a predominant north/south relative motion as was shown above in Fig. 7.

Fig. 14 and 15 characterize close approach relative velocity at TCA as a function of longitude and inertial right ascension, respectively. The longitudinal dependencies are evident in that the active GEO satellites being screened are only occupying certain longitudinal bands (e.g. North America and Europe/Middle East/Asia). While the longitudinal dependency (Fig. 14) indicates increased conjunction likelihood near the Earth's gravity wells at 75° E and 105° W, it is unclear how much of this is due to recurrent debris at the gravity wells versus the fact that the 292 GEO satellites for which we receive CDMs are simply located near those gravity wells, leading to potential misperception of more (or

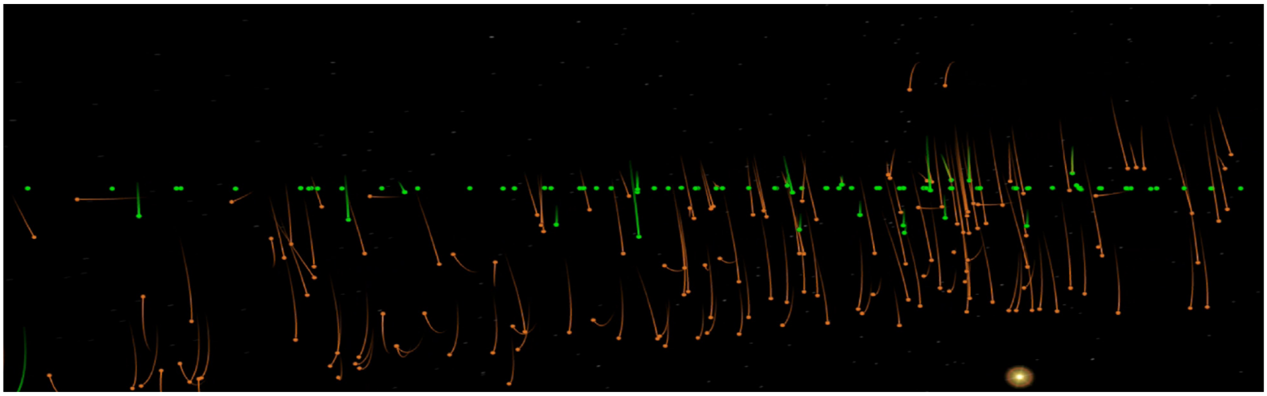

Fig. 7. Typical active GEO satellite-vs-inclined debris approach paths as viewed from within the equatorial plane looking radially outward. Green dots are active GEO satellites and orange dots are current GEO debris. (For interpretation of the references to colour in this figure legend, the reader is referred to the Web version of this article.)

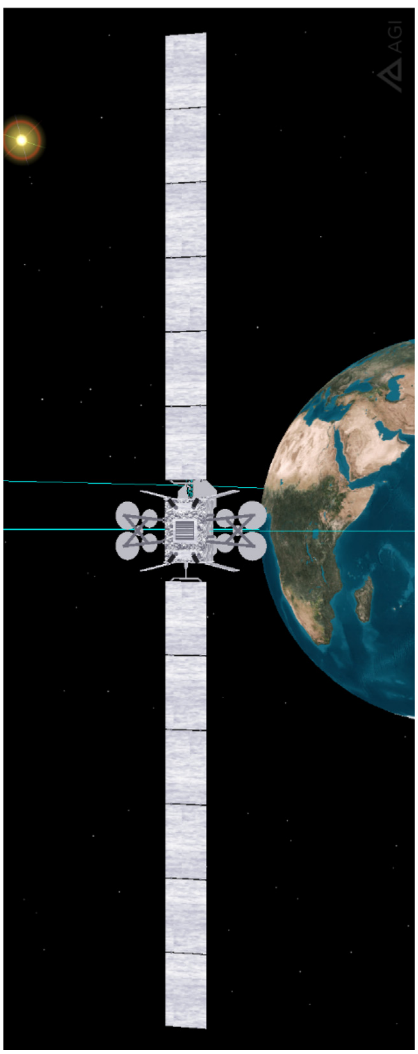

Fig. 8. Boeing 702 satellite, viewed from above (nearly normal to solar panels).

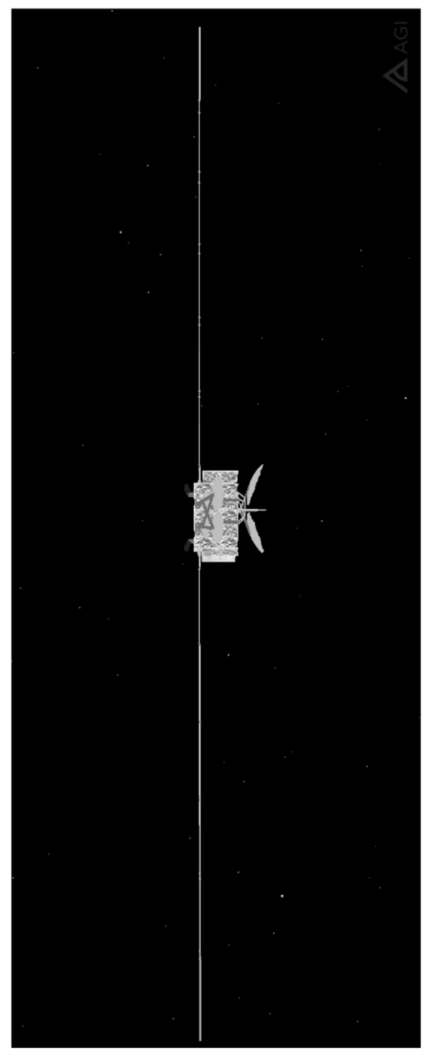

Fig. 9. Boeing 702 satellite, viewed from east looking west.

less) collision risk.

With its distinctive sinusoidal shapes and high relative velocities, it's worthwhile to forensically examine the constituent secondary objects which in aggregate lead to Fig. 15, as shown in Fig. 16. Note the conjunctions having relative velocities higher than 3 km/s.

The type of secondary orbits comprising these conjunctions is shown in Fig. 17. This is a complementary breakdown of GEO collision risk to that contained in Fig. 1 of Anderson/Schaub [18].

The GEO ± 100 km altitude-crossing orbit population in today's public catalogue is depicted in Fig. 18, with volumetrically-enhanced spatial density representations in Fig. 19. The camera viewpoint of Fig. 18 is in the X-Y plane of the inertial frame, looking directly down the X-axis (i.e., from the vantage point of inertial right ascension = 0°). In Fig. 19, the yellow vector points toward an inertial right

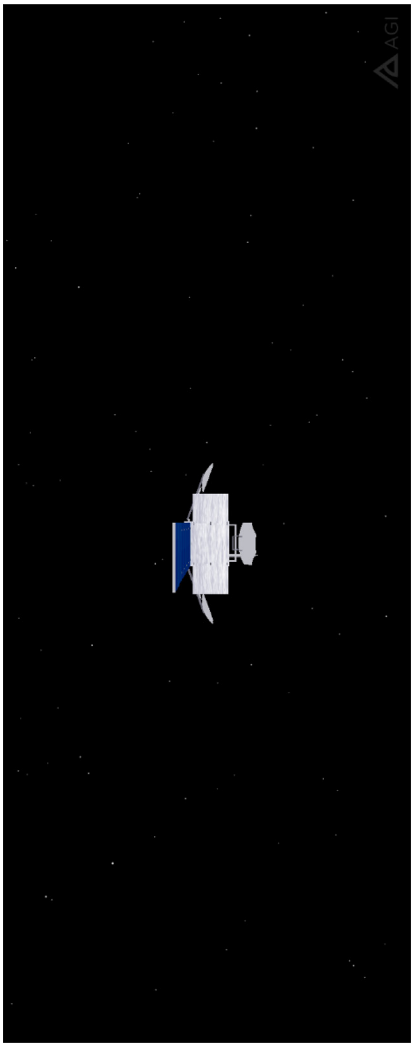

Fig. 10. Boeing 702 satellite, viewed from north looking south (lengthwise, along solar panel).

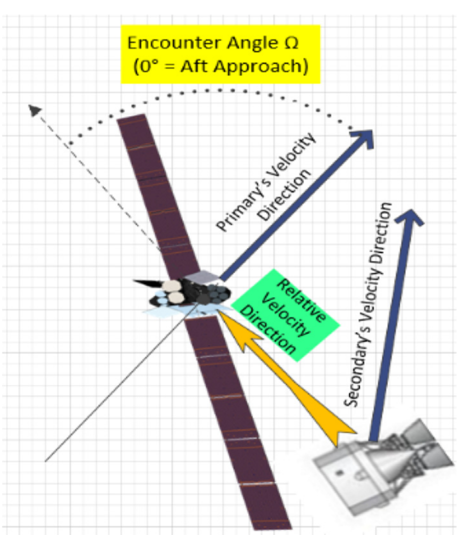

Fig. 11. Close approach relative velocity encounter angle.

ascension = 0°, and the magenta and green vectors point to −60° and +60° degrees in right ascension, respectively. From these figures it can be seen that the ensemble of ascending nodes occupied by the inclined

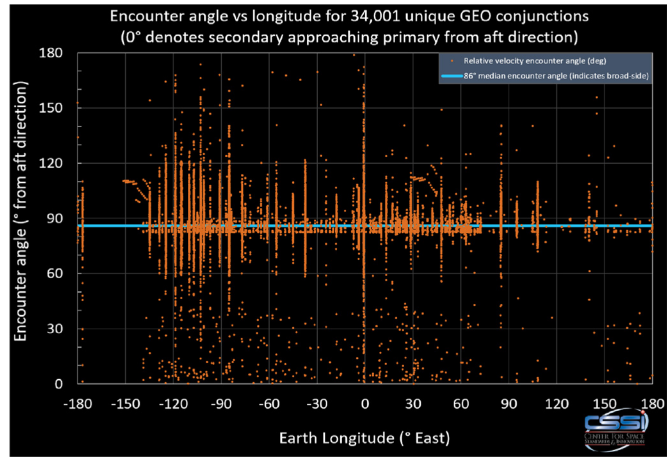

Fig. 12. Close approach relative velocity encounter angle vs. Earth longitude.

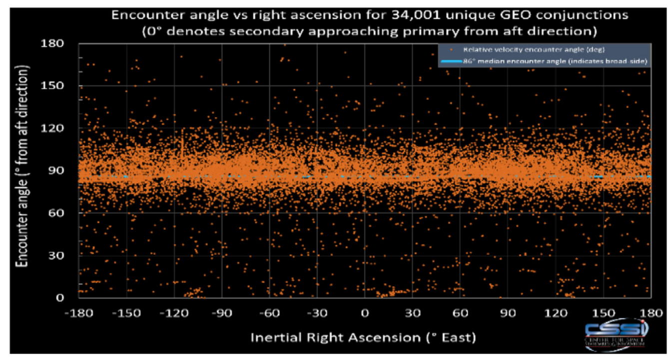

Fig. 13. Close approach relative velocity encounter angle vs. inertial right ascension.

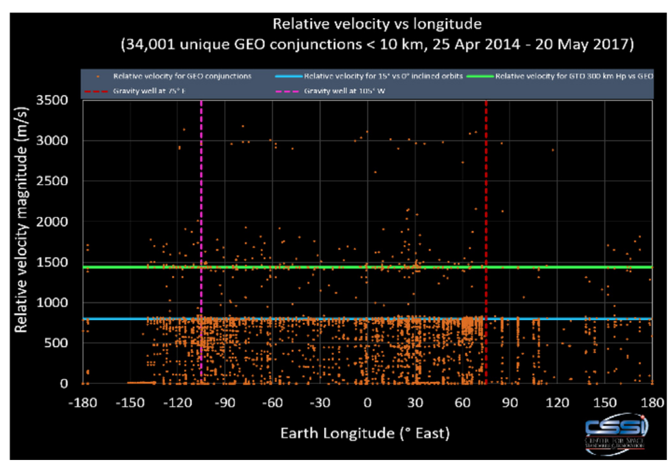

Fig. 14. Close approach relative velocity vs. Earth longitude.

debris fragments is centred at 0° spanning ± 60°.

This range of ascending nodes represents the collective third-body perturbations-induced evolution of the inclination vector in phase space about an ascending node of 0° and inclination of 7.3° as explained by Chao [19] and profiled by Nazarenko [20] (Fig. 20, updated in Fig. 21). That there is no apparent dependence of relative velocity upon longitude (Fig. 14) is consistent with Soop [21].

Evolution of the inclination vector in its 53-year cycle is responsible for the sinusoidal relative velocity trend below 800 m/s in Fig. 16, since orbit inclination for debris objects decreases the further right ascension of the ascending node is from 0°. To see this more clearly, we employ

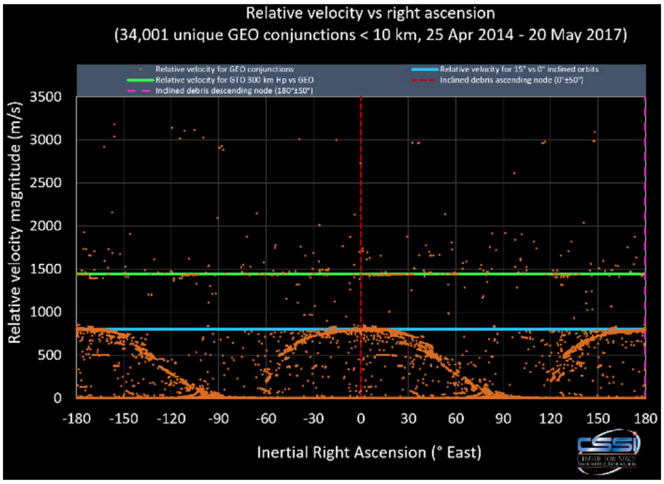

Fig. 15. Close approach relative velocity vs. inertial right ascension.

the "ring method" to assess relative velocity and orbit inclination of catalogued objects that pierce an equatorial altitude ring centred on GEO altitude, as a function of right ascension of the piercing location, yielding Fig. 22 and Fig. 23. Note that when using TLE mean orbital elements in the ring method, those elements can be used to calculate mean radius r_{mean} at the ascending and descending nodes, but this must then be converted to osculating radius (Eq. (29) of [37]) via:

$$r_{osc} = r_{mean} + \Delta r \tag{4}$$

$$r_{osc} = r_{mean} + \frac{J_2 R_E^2}{p}\left[-\frac{1}{2}\left(1 - \frac{3}{2}\sin^2 i\right)\left(1 + \frac{e\cos\nu}{1+\sqrt{1-e^2}} + \frac{2r}{a\sqrt{1-e^2}}\right) + \frac{1}{4}\sin^2 i\cos(2\nu + 2\omega)\right] \tag{5}$$

which simplifies at ascending and descending nodes to:

$$r_{osc} = r_{mean} + \frac{J_2 R_E^2}{p}\left[-\frac{1}{2}\left(1 - \frac{3}{2}\sin^2 i\right)\left(1 \pm \frac{e\cos\omega}{1+\sqrt{1-e^2}} + \frac{2r}{a\sqrt{1-e^2}}\right) + \frac{1}{4}\sin^2 i\right] \tag{6}$$

The plus sign corresponds to the ascending node and minus sign to the descending node. All independent variables are mean orbit elements (i.e. prior to addition of the short-periodic perturbations in the conversion from mean to osculating).

Note the direct correlation of the sinusoidal trends in relative velocity caused by debris orbit inclination of the piercing debris.

Hansen/Sorge conducted a similar statistical aggregation of conjunction statistics in Ref. [22] using a year-long conjunction data set, from which they'd concluded that relative GEO velocities would not exceed 1 km/s. The significantly higher observed relative velocities of up to 3.2 km/s in Fig. 16 (extracted from actual JSpOC CDMs for conjunctions < 10 km) were likely detected because of the larger GEO conjunction dataset we used. This three-to four-fold increase in relative velocity is consistent with [23] and indicates a higher level of collision lethality and subsequent collision risk than had been previously anticipated. Further examination revealed that these higher relative velocity secondaries in Fig. 23 were a subset of the "400 GTO and high-eccentricity debris" category.

The relative velocity between GEO and GTO orbits, depicted in Figs. 14–16 by a horizontal green line, was assessed as shown in Fig. 24 as a function of orbit inclination and GTO perigees of 300, 400, and 500 km with apogee set at GEO altitude. The Hohmann transfer velocity vectors at various inclinations were then differenced from the GEO velocity vectors to obtain the relative velocities as portrayed in Fig. 24 below.

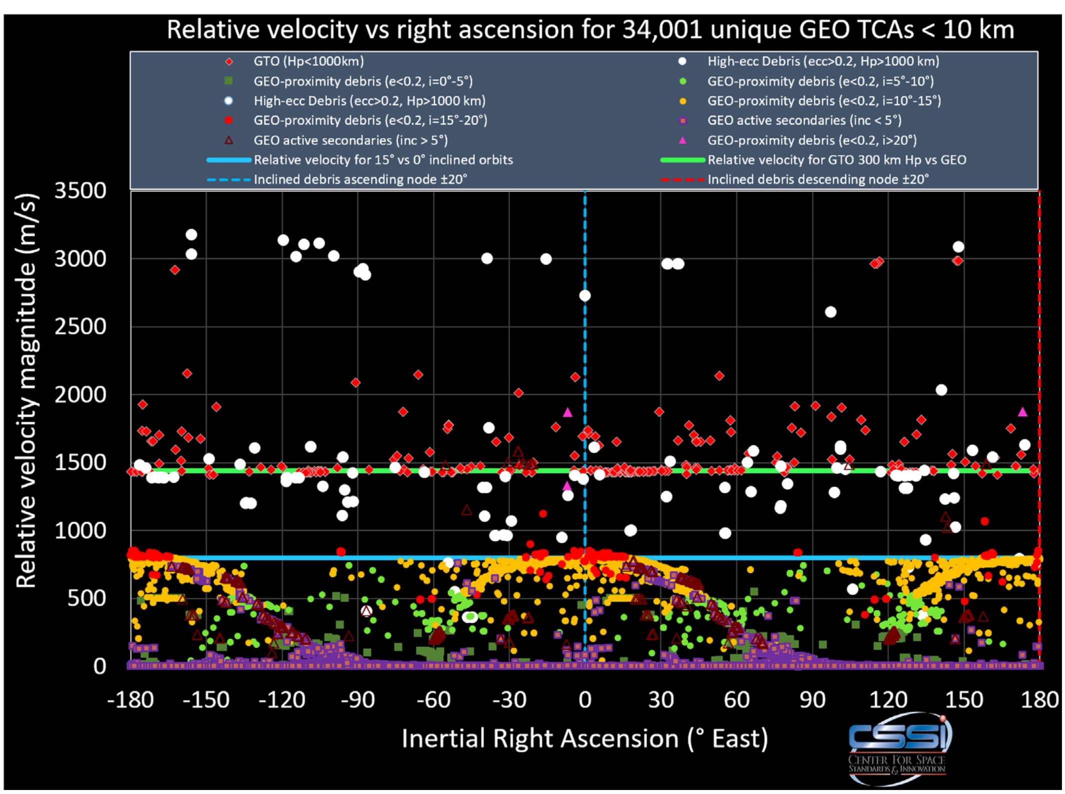

Fig. 16. Detailed forensics of relative velocities for 34,009 JSpOC close encounters by secondary (conjuncting) object orbit type.

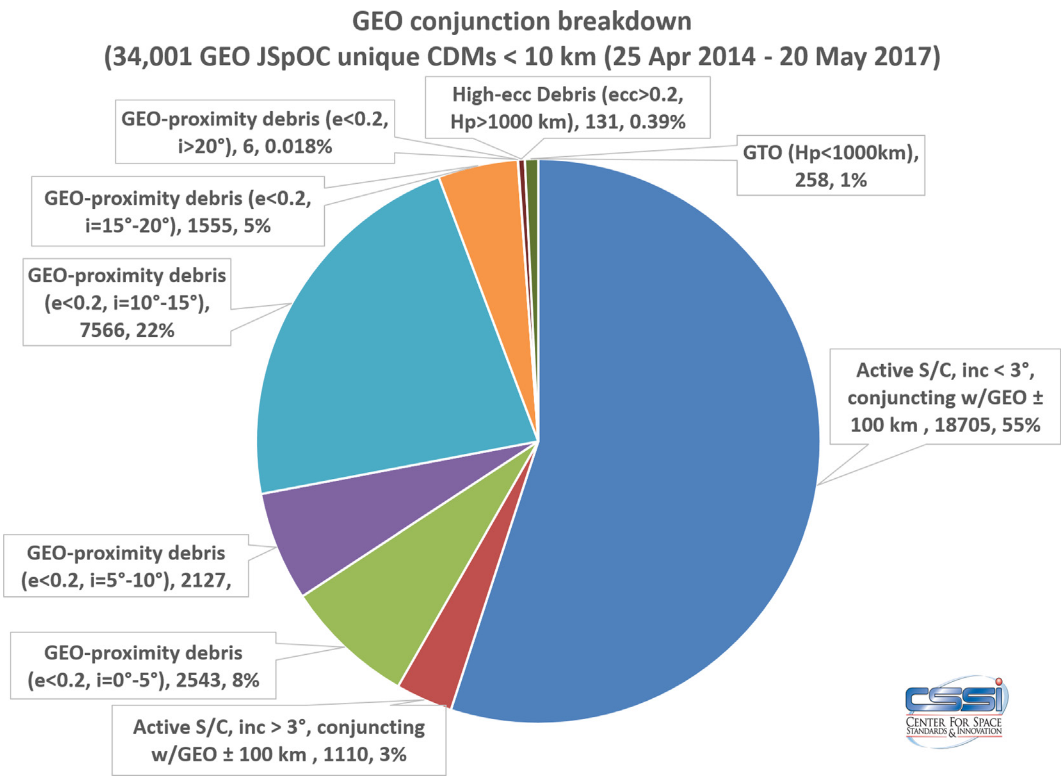

Fig. 17. Characterization of 34,009 JSpOC close encounters by secondary (conjuncting) object type. Half of these secondaries are active GEO satellites, which may include inter-operator intentional collocations, potentially skewing this statistic.

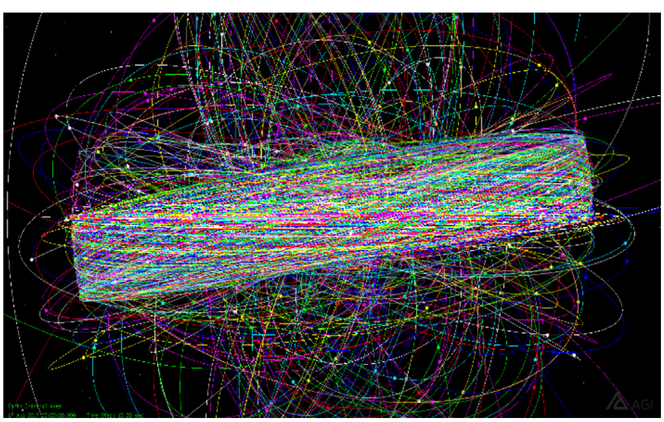

Fig. 18. All GEO ± 100 km altitude-crossing objects viewed from the Vernal Equinox direction.

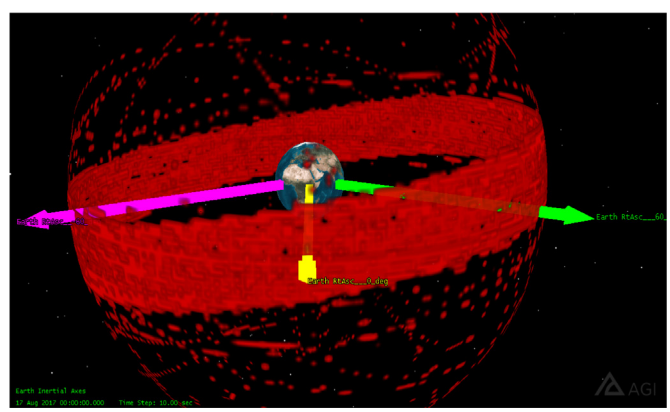

Fig. 19. Equivalent 3D spatial density volumetric of all GEO ± 100 km altitude-crossing objects, including vector aligned with Vernal Equinox (yellow) and two vectors in equatorial plane 60° away. (For interpretation of the references to colour in this figure legend, the reader is referred to the Web version of this article.)

4.2. Collision rate multiplier accounting for non-broadside conjunctions

As justified in the previous section, we will be assuming a collision with a 1 m radius (presumed spherical) debris fragment will occur at a miss distance at TCA of 5 m. This allocates a cross-sectional radius of 4 m for the primary satellite. Using this combined 5 m distance, collision rates will be estimated.

The CDM statistics of Figs. 12 and 13 allow a further refinement of this single miss distance-based collision rate estimate. Since collision probability scales approximately linearly with cross-sectional area, we can construct a simple area blending function with independent variable η. For a Boeing 702 satellite with a roughly 6 × 8 m cross-section viewed along the north/south direction and roughly 42 × 6 m as viewed along the east/west direction, and noting that the inertial Z-component $\widehat{V_{rel}}_z$ of the inertial relative velocity unit vector approximates $\cos\eta$, the satellite's cross-sectional area in the encounter plane can be approximated by:

$$Area_{702}(\eta) \approx (42 \times 6) - \cos\eta\,[(42 \times 6) - (6 \times 8)] \tag{7}$$

By applying this cross-sectional area approximation to all 34,009 unique GEO ± 100 km conjunctions and averaging, a CDM-ensemble-averaged asymmetrical collision rate scaling factor SF can be computed as:

$$SF_{Off-N/S} = \frac{\sum_1^{N_{CDM}} [Area_{702}(\eta) + \pi r_{secondary}^2]}{(N_{CDM})[(6 \times 8)_{N/S} + \pi r_{secondary}^2]} = 1.29 \tag{8}$$

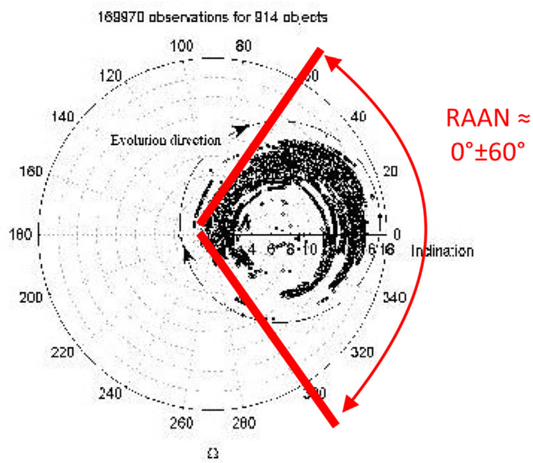

Fig. 20. Inclination vector in phase space for 914 GEO RSOs (Fig. 4.4 from Ref. [20], included by permission of author).

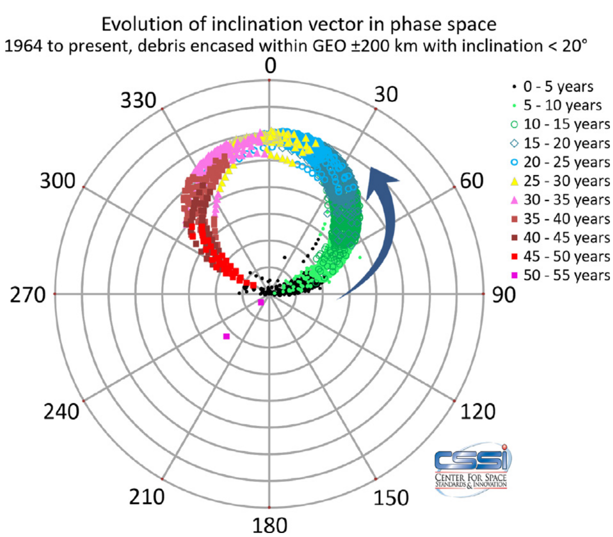

Fig. 21. Refresh of Nazarenko's inclination vector in phase space for period 1964 to present, all debris encased by GEO ± 200 km with inclination < 20°. Colours denote how far into cycle the RSO's evolution was at that time. (For interpretation of the references to colour in this figure legend, the reader is referred to the Web version of this article.)

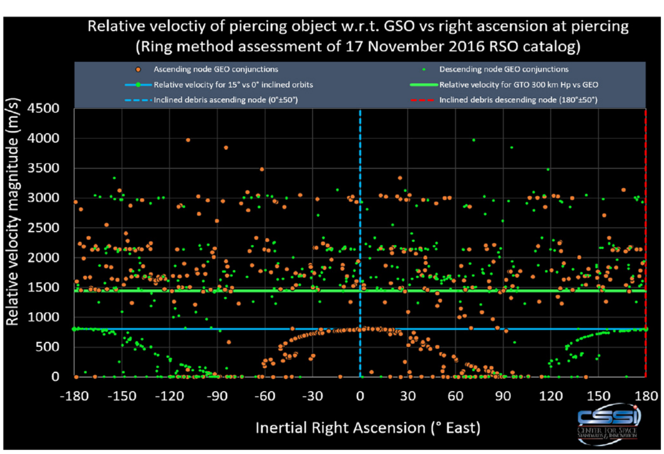

Fig. 22. Relative velocity of catalogued objects piercing a GEO ± 100 km ring vs right ascension.

5. GEO collision likelihood and encounter rate estimation techniques

Techniques used to estimate encounter rate or likelihood fall broadly into one of three types:

(1) Spatial density, or flux-based, methods [8,24–26,32,35,40]. In this approach, a flux-based Annual Collision Probability (ACP) approach is employed to estimate collision likelihood.
(2) Encounter rate characterization via numerical simulation approaches [27–30,32].
(3) Operationally-based close approach statistics [34].

As will soon be discussed, while the spatial density/flux method may be an effective collision likelihood estimation tool in the LEO regime, the method is likely ill-suited if not potentially fatally flawed for GEO collision rate analysis due to the high flux variability in altitude, longitude, latitude and even inertial right ascension. Typical analyst assumptions that the primary satellite flies thru a static, positionally-uncorrelated density of “other” objects is also likely flawed in the GEO (synchronous) regime.

Methods #2 and #3 are problematic as well, because direct estimation of average collision rate via numerical techniques would require too massive a quantity of samples (e.g. from a Monte Carlo simulation or from operational conjunction assessment results) in order to obtain a statistically-relevant ensemble of collision data. As an extreme case, consider that a Monte Carlo conjunction run sufficient to reliably estimate the likelihood of a collision occurring between two 1U CubeSats (i.e., two cubes, each sized 10 × 10 × 10 cm) may have to cover an analysis span of millions of years (by which time the simulation conditions have substantially changed, nullifying the estimate).

6. External research to date relevant to GEO collision likelihood and encounter rate estimations

Other researchers have attempted to quantify GEO collision likelihood or at least to characterize the relationship between encounter radii and encounter rates.

Since the log (#annual encounters) vs log(miss distance) plot format has proven useful in the LEO regime [39], we will use that format for characterizing collision and encounter rates throughout this paper. As was mentioned in the introduction, these characterizations will be “normalized” to 167 SDA Big 4 satellites for comparative purposes; the accuracy of such a normalization is discussed later. Without normalization, relevant external research is captured in Fig. 25.

In this section, the focus is to extract any/all relevant collision likelihood estimates in order to map those estimates into an SDA Big 4 set of 167 satellites and the GEO active satellite and debris population of 2017.

6.1. GEO collision likelihood external research

First, external research into the likelihood of hardbody collision is examined. To help reduce the number of plots (and page count) of this paper, all such external research to estimate GEO collision likelihood is amalgamated into Fig. 28. A quick examination of this figure shows that there is at present much disagreement regarding GEO collision risk.

6.1.1. Aerospace Corporation 2004

Peterson [29] generated 87 weeks of conjunction assessment statistics for more than 400 active GEO satellites, with 130,000 resulting conjunctions to characterize residual (unmitigated) collision risk as a function of data quality (his Fig. 4, presented as Fig. 26 in this paper). Per correspondence with Peterson, he stated that his figures correspond to the “active satellites-on-all” case, contrary to his last paragraph of the methodology section, which states that “*The primaries consisted of all*

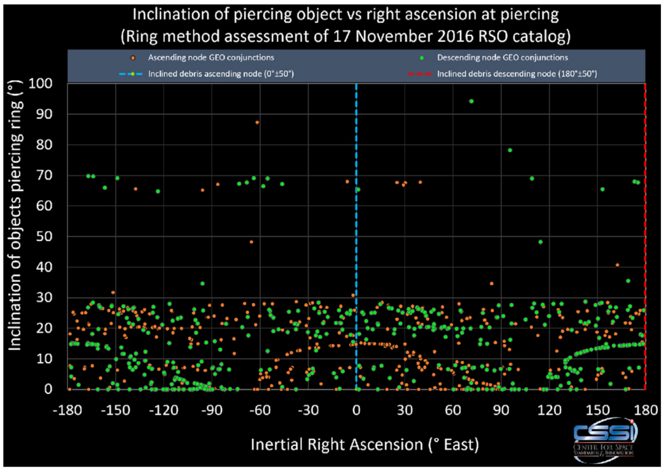

Fig. 23. Inclination of catalogued objects piercing a GEO ± 100 km ring vs right ascension.

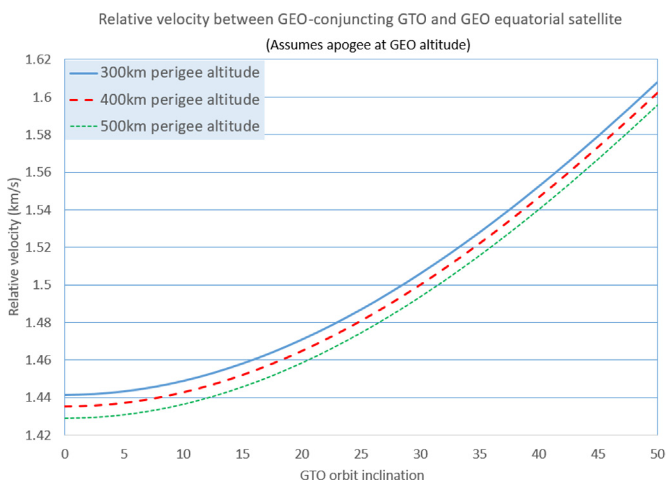

Fig. 24. Relative velocity between GEO equatorial satellite and GEO-conjuncting GTOs with 300, 400 and 500 km perigee altitudes.

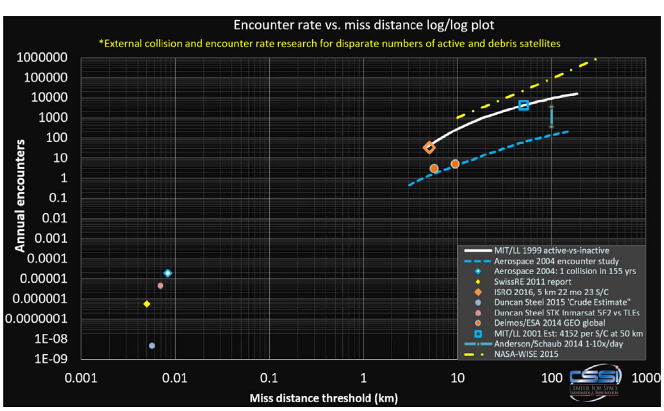

Fig. 25. Unadjusted, unnormalized collision and encounter rate estimates from external researchers.

objects (satellites and debris).".

Peterson varied collision probability avoidance manoeuvre threshold for various combinations of primary and secondary object accuracy to assess "total risk per satellite over a 10 year mission". Peterson astutely noted that convergence of the various orbit quality combinations to a single value allowed him to identify the probability of collision if no avoidance action were taken (equalling the total 87-week collision risk result).

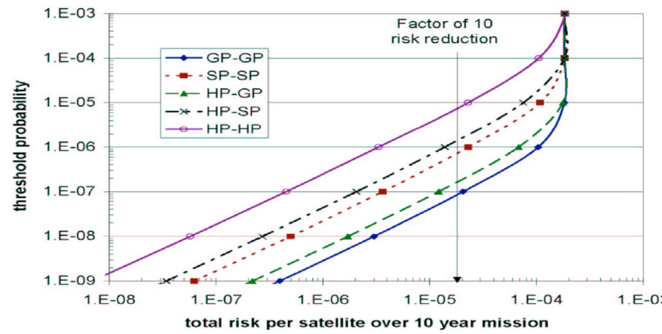

Fig. 26. Peterson's "Fig. 4: Variability in threshold probability for individual conjunctions as a function of total mission risk" (included by permission of author).

Peterson stated that in 2004 there were 465 (225 + 300-60) active satellites. In 2005, there were 938 RSOs passing through a GEO ± 100 km shell (from which 473 inactive RSOs must have "passed through GEO (938-465). In 2017, using that same GEO shell-passing filter, there are 478 active and 888 debris RSOs.

He assumed a 10 m hardbody dimension (i.e., radius of 5 m) for the primary satellite, with the secondary object size derived from an internal satellite size database (which presumably defaults to 6.673 m for debris [31]), for a total combined hardbody radius of 8.34 m.

Consequently, his Fig. 4-identified annual collision likelihood of $1.85{*}10^{-5}$ per satellite can be mapped to 167 satellites and 2017 RSO catalogue population conditions as:

$$\frac{\#Big4\ collisions}{yr}_{2017} = \left[\frac{1.85e-5}{yr}\right]_{per\frac{S}{C}} 167_{SDA}\left[\frac{478_{2017}}{465_{2004}}\right]_{debris}\left[\frac{888_{2017}}{473_{2000}}\right]_{debris}$$
$$= 0.00596 \text{ per year} \tag{9}$$

This result is plotted in Figs. 25 and 28 as "Aerospace 2004: 1 collision in 155 yrs".

6.1.2. Duncan Steel, blog posts, 2015

This researcher has authored a number of blog posts to estimate collision likelihood in both the LEO and GEO regimes. In Ref. [32], he presented results obtained from two estimation techniques.

In his analysis he assumed that all controlled objects in GEO will not collide with each other. For the remainder of the collision risk, he took a self-described crude approach in computing the probability of a GEO satellite encountering a Geosynchronous Transfer Orbit (GTO) object. He considered a geocentric sphere with radius equal to the distance of the geostationary band (approximately 42,000 km). Such a sphere would have a surface area of $4\pi r^2$ ($2.217{*}10^{-16}\ m^2$). By estimating the combined cross-section of the conjuncting satellites to be 100 square meters (circle of radius 5.642 m), projecting this area on to the sphere's surface twice per GTO orbit, and considering such an orbit will have a period less than one sidereal day (perhaps about 15 h), he arrived at an encounter rate for a single GTO versus a single GEO.

$$\frac{\#Enc_{Single\ GTO,GEO\ pair}}{yr} = \left[\frac{2_{crossings}}{rev}\right]\left[\frac{24\ revs}{15\ days}\right]\left[\frac{100\ m^2}{4{*}\pi{*}42000000^2 m^2}\right]\left[\frac{365.25\ days}{yr}\right]$$
$$= 5.273{*}10^{-12} \tag{10}$$

We assume that the author used the term "GTO" to represent any high-eccentricity GEO-crossing satellite. Assuming 888 GTO satellites traversing the GEO ± 100 km altitude range conjunct with 167 GEO satellites (5.642 m radius each) the resulting encounter rate (Fig. 28, "Duncan Steel 2015 "Crude Estimate") is

$$\frac{\#Enc_{All\ GTO,GEO\ pairs}}{yr} = 888_{GTOs}167_{SDA}5.273{*}10^{-12} = 7.819{*}10^{-7} \tag{11}$$

As will be demonstrated, this rate is low and out of family with most other results, perhaps because GTO tracks are not uniformly distributed about the geocentric sphere. By design, GTOs will only cross a very narrow equatorial band on the sphere; therefore the entire sphere's surface area should not be considered.

Without elaboration, he also stated that by examining the TLE catalogue for INMARSAT-5F2 conjunctions, the net collision probability per square meter per year is $3.06{*}10^{-8}$. Applying the same methodology as above with an area of 150 square meters (circle of radius 6.91 m) we arrive at the annual value (Fig. 28, "Duncan Steel STK Inmarsat 5F2 vs TLEs") of:

$$\frac{\#Enc_{All\ GTO,SDA\ pairs}}{yr} = 150_{Area}167_{SDA}3.06{*}10^{-8} = 7.6653{*}10^{-4} \tag{12}$$

Based on his two analyses he concluded that collision probability is so low for GEO active satellites against GEO debris that it is unreasonable to deorbit (i.e., to super-sync) GEO satellites at their end of life. However, one need only examine the pie chart breakdown of the JSpOC operational conjunctions detected (Fig. 17) to see that non-GTO collision likelihood comprises a large percentage of existing CDMs.

6.1.3. SwissRE report, 2011

This online publication [24] incorporates results from analyses later published in Ref. [8]. This characterization of the likelihood of collision in GEO employed a KGT (spatial density or flux) technique. Specifically, the author's Fig. 8 of [8] (Fig. 27 in this paper) characterizes per-satellite annual collision likelihood for equatorial GEO active satellites. In correspondence with the author, he used a cell size of 736 km × 736 km × 400 m with an area of 100 m^2 and a relative velocity of 500 m/s.

As stated in Fig. 8's caption in Ref. [8], "*The collision hazard … produces a probability of collision that is lower than previous calculations.*" As will be shown, this collision likelihood estimate is among the lowest of any method examined herein. By digitizing this curve, evaluating the Pc (from the curve) for 416 current GEO equatorial satellites, and properly combining the results, an annual likelihood of $5.47931{*}10^{-7}$ was obtained, which can be mapped to 167 SDA satellites (Fig. 28, "SwissRE 2011 report") as:

$$\frac{\#Enc_{167\ SDA\ GEOs}}{yr} = [5.47931{*}10^{-7}]_{416}\left[\frac{167_{SDA}}{416_{GEO\ eq}}\right] = 2.1996{*}10^{-7} \tag{13}$$

6.2. GEO encounter rate external research

Next, relevant external research characterizing how encounter rates vary with miss distance is examined. To help reduce the number of plots (and page count) of this paper, all such external research to estimate GEO collision likelihood is amalgamated into Fig. 33.

6.2.1. MIT/Lincoln laboratory reports, 1999 and 2001

LeClair [27,28] estimated in 1999 that the 270 GEO active satellites would encounter the 430 inactive geosynchronous objects 4152 times per year to within 50 km miss distance.

As of 26 August 2017, the number of GEO-crossing (GEO ± 200 km) objects has grown to 480 active GEO satellites and 1037 inactive debris objects. Accordingly, LeClair's estimated 50 km encounter rate can be approximately mapped to the SDA Big 4's 167 S/C and 2017 GEO debris and active satellite populations as:

$$\left.\frac{\#Enc_{50km}}{yr}\right|_{2017} = \left[\frac{167_{2017\ SDC\ Big\ 4}}{270_{1999}}\right]_{actives}\left[\frac{1037_{2017}}{430_{1999}}\right]_{debris} 4152 = 1.49 \times 4152 = 6193 \tag{14}$$

Upon further exploration, Fig. 2 of LeClair's paper also presents the full PDF of annual encounters as a function of miss distance. Applying the above scaling factors to the resulting trend yields the "MIT/LL 1999 active vs inactive" line in Fig. 33.

6.2.2. Aerospace Corporation 2004

Peterson [29] similarly characterized the number of encounters that a single GEO active satellite is likely to experience in one year of operations in Fig. 3 of that paper (Fig. 30) here. This trend was obtained by conducting conjunction analysis of over 400 GEO active satellites against the public TLE catalogue over an 87-week simulation period. Digitizing that curve and again scaling by the following yields Fig. 33, "Aerospace 2004 encounter study":

$$\left.\frac{\#Enc}{yr}\right|_{2017} = [Fig.\ 3]_{per\frac{S}{C}}\, 167_{SDA}\left[\frac{478_{2017}}{465_{2004}}\right]_{actives}\left[\frac{888_{2017}}{473_{2004}}\right]_{debris} \tag{15}$$

6.3. Indian Space Research Organization, 2017

Indian Space Research Organization (ISRO) currently has 23 operational spacecraft [33] in Geostationary (GEO) and Geosynchronous (GSO) orbits. Kannan et al. [34], listed all encounters within 5 km for those operational GEO/GSO spacecraft for approximately 22 months during the years 2015 and 2016, totalling 33 encounters. The resulting average encounter rate of 0.7174 per year per satellite was mapped to the 167 satellites of initial interest in this paper resulting in an estimated 131 encounters per year (Fig. 33, "ISRO 2016, 5 km 22 mo 23 S/C") via:

$$\frac{\#Enc_{5\ km}}{yr} = \left[\frac{33\ enc_{5\ km}}{1.82888\ years}\right]\left[\frac{167_{SDC\ Big\ 4}}{23_{ISRO\ S/C}}\right]_{actives} = 131 \tag{16}$$

6.4. Deimos/ESA spatial density-based estimate

Sanchez-Ortiz et al. [35], evaluated conjunctions of two spherical objects, the first (primary) with a radius of 2 m and the other (secondary) with a 1 m radius. For the GEO case in Fig. 31 (labeled as Fig. 28 in Ref. [35]), the authors indicate that a GEO satellite will experience 3 encounters per year per satellite having a collision probability of $1{*}10^{-7}$. Each of the objects was assumed to have a 1-sigma variance of 2.5 km in all directions, from which we have inferred a miss distance of 5.64 km. Mapping their estimated average encounter rate of 3 per year per satellite to the 167 SDA satellites of interest in this paper results in 501 encounters per year. In like fashion, the 5 encounters they

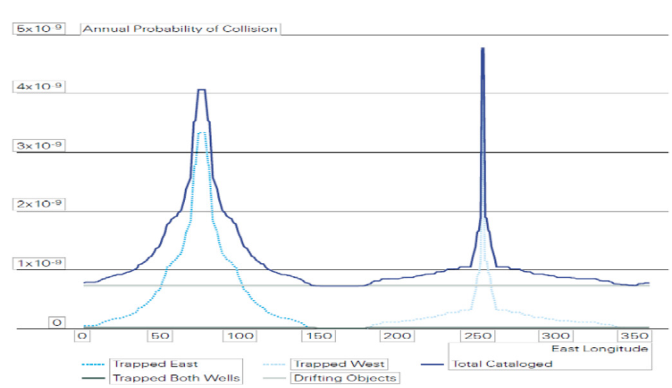

Fig. 27. Flux-based estimate of GEO collision likelihood [24] (included by permission of author).

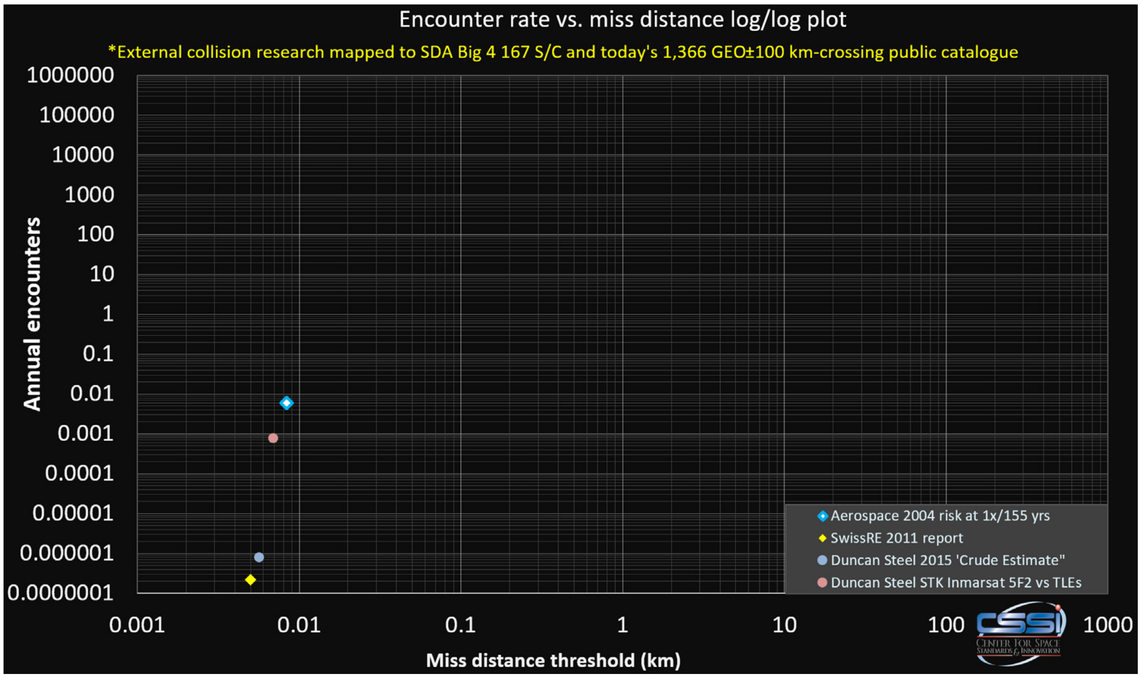

Fig. 28. Relevant external research on estimated collision likelihood, mapped to 167 "SDA Big 4" satellites and a 2017 JSpOC catalogue containing 1366 GEO ± 100 km-crossing RSOs.

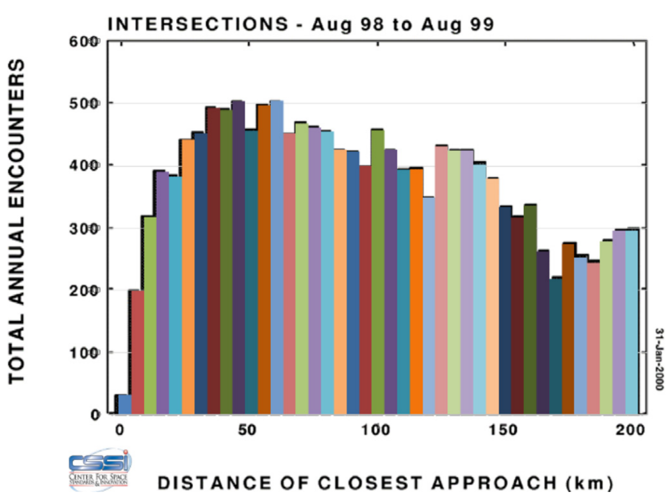

Fig. 29. Digitization of MIT/LL (LeClair's) Fig. 2, entitled "Distribution of Encounter Distance of Closest Approach" (included by permission of author).

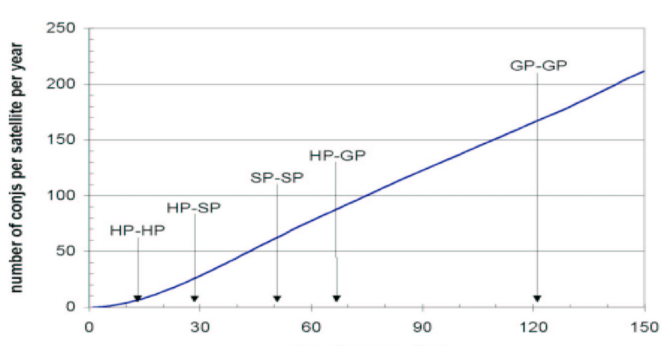

Fig. 30. Peterson's "Number of times per year that a given miss distance is violated" (included by permission of author).

estimated corresponding to a $1*10^{-8}$ collision probability maps to 835 encounters per year. These are denoted, "Deimos/ESA 2014 GEO global" in Fig. 33,. We were not able to infer a miss distance associated with $1*10^{-6}$ or $1*10^{-5}$ because a zero miss distance with variance 2.5 km for a 3 m combined radius only produces a probability of $3.6*10^{-7}$.

6.5. NASA-WISE study

The NASA Wide-Field Infrared Survey Explorer (WISE) increased the current catalogue of known debris by radiometrically measuring debris in near Earth orbit [12]. Based on this revised debris estimate, the total collisional rate in the GEO belt was estimated. Although not specified, it is our interpretation that the collision rates depicted in their Fig. 5 (shown here as Fig. 32) were for a 2017 active GEO population of approximately 478 satellites against debris. Their simulation timespan of 5 days yielded the number of conjunctions occurring within that timespan as a function of screening distance.

A yellow dash-dotted line entitled "NASA-WISE 2015" in Fig. 33 was obtained from:

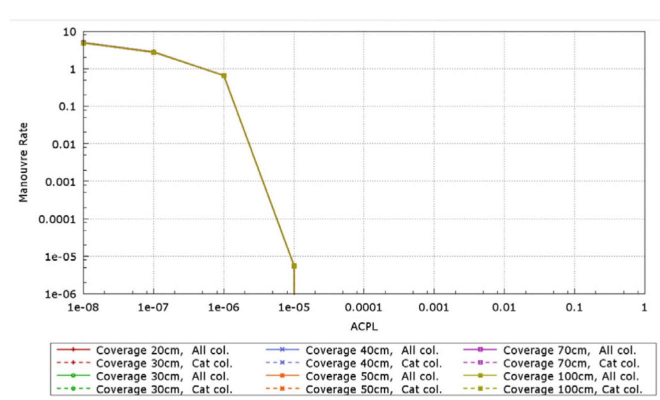

Fig. 31. Fig. 23, extracted from Ref. [35] (included by permission of author).

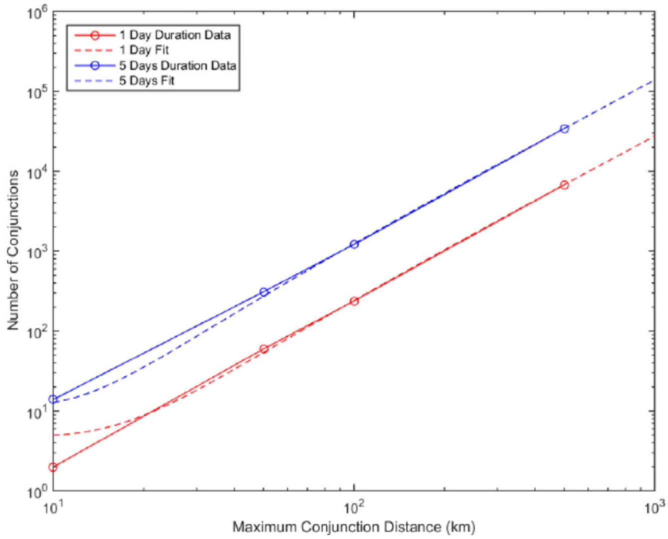

Fig. 32. "Number of conjunctions of the 2011 catalog with debris vs [minimum] conjunction distance in km for a 1-day time frame (red) and a 5-day time frame (blue)". (included by permission of author). (For interpretation of the references to colour in this figure legend, the reader is referred to the Web version of this article.)

$$\left.\frac{\#Enc_{\text{NASA WISE}}}{yr}\right|_{2017} = \left[\frac{\#Enc_{\text{NASA WISE}}}{5\ days}\right]\left[\frac{167_{2017\ SDC\ Big\ 4}}{478_{2017}}\right]_{actives}\left[\frac{365.25\ \text{day}}{1\ yr}\right] \tag{17}$$

6.6. University of colorado study

Anderson and Schaub [30,36] have done extensive investigations into on-orbit evolution and dynamics of fragments introduced into the GEO arc. Their focus has been primarily to characterize that motion, and subsequent collision risk, as a function of longitude.

As part of (and a precursor to) that study, they conducted a 5-year macroscopic congestion forecast "using a minor radius of 100 km and the GEO debris population in the 08/28/2013 TLE data set to evaluate current levels of background noise in this ring." They assumed that controlled satellites would maintain their designated longitudinal slots, while the 750 uncontrolled debris objects would be propagated forward freely in time.

In preparatory comments to the main GEO longitudinal fragmentation dynamics characterizations which are the focus of their research, the authors anecdotally state that "controlled satellites in the longitude slots neighbouring the gravitational wells are subject to 6–10 near-miss events per day at a distance of 100 km … and a maximum of 1–2 near-misses per day at 100 km"

The insights of these preparatory comments were incorporated into Fig. 33, "Anderson/Schaub 2014 1-10x/day" by simply selecting the two bounding limits (i.e., a low value of 1 and a high of 10), and scaling via:

$$\left.\frac{\#Enc_{\text{Univ of CO}}}{yr}\right|_{2017} = [1\ or\ 10\ per\ sat][167_{SDC\ Big\ 4}]\left[\frac{365.25\ \text{day}}{1\ yr}\right]\left[\frac{478_{2017}}{468_{2013}}\right]_{actives}\left[\frac{888_{2017}}{750_{2013}}\right]_{debris} \tag{18}$$

7. Material and methods: encounter rate evaluation fundamentals

As noted above, there are three basic approaches to assessing encounter rates; within the encounter rate simulation category is the volumetric encounter rate method developed by the authors [37,38]. Although this volumetric encounter rate approach was not originally designed for synodic, correlated relative motion (i.e., geosynchronous orbits), nevertheless it is instructive to review this approach to gain a better understanding of what drives encounter rates as a function of miss distance.

As presented in our LEO encounter rate characterization paper [39], in order for two satellites to "encounter" each other to within a specified miss distance, the product of two linear relationships leads to a squared relationship:

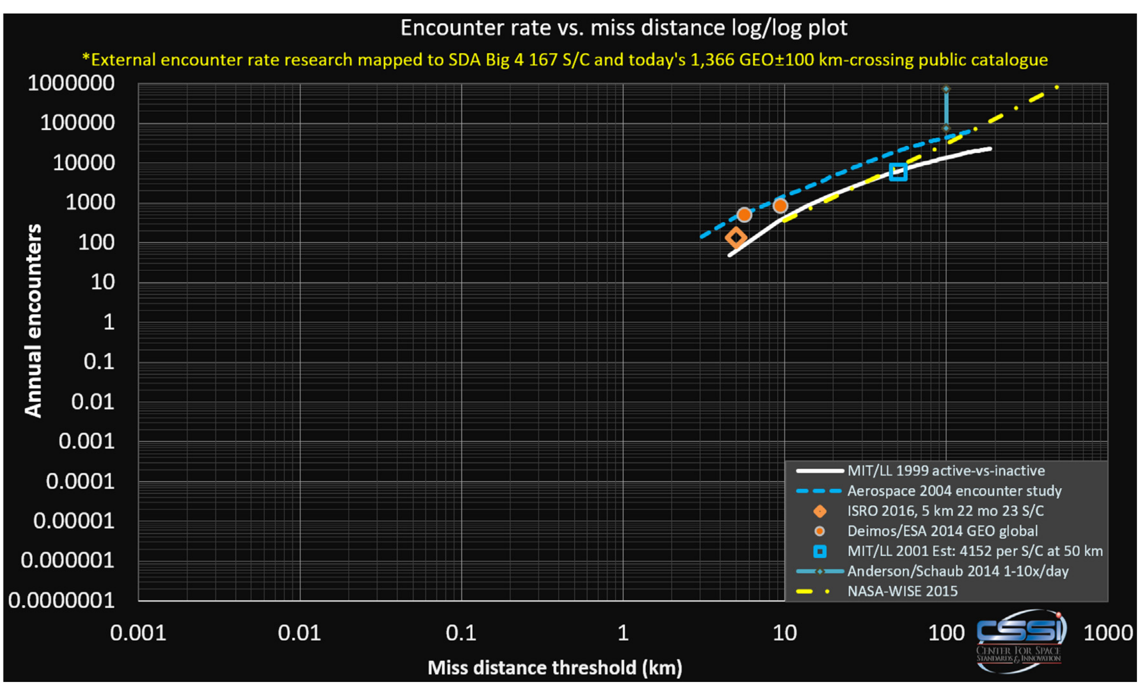

Fig. 33. Relevant external research characterizing estimated encounter rate, mapped to 167 "SDA Big 4" satellites and a 2017 JSpOC catalogue containing 1366 GEO ± 100 km-crossing RSOs.

- "The two (primary and secondary) trajectories must be capable of touching to within the tolerance of the encounter radius R_E", in which case "the number of trajectories (assuming a dense supply of non-synodic possible conjuncting orbits) is a linear relationship with R_E."
- For conjuncting orbit pairs (i.e., that have non-zero volumetric collision probability), the rate of encounter is a direct function of the orbit progression through MA1, MA2 phase space (Fig. 34) … [thereby varying] linearly with R_E.

An alternate, simplified way to think about it is that for two objects to collide, they must be on trajectories that can collide, and they must both transit that collision region at the same time. So the two constituent sub-relationships are:

1. Increasing R_E linearly admits more RSOs having encounter potential with neighbouring altitude bands
2. When encounter potential already exists, increasing R_E linearly increases encounter rate

Yielding: $$\left[\frac{\#\ encounters}{time}\right] \propto [R_{encounter}^2] \tag{19}$$

7.1. Equivalences between encounter rates and "time between molecular collisions in gas dynamics & R_E^2 relationship

As was previously shown, encounter rate in higher-density, non-synodic (non-GEO) regimes approximately varies in proportion to the encounter screening radius. This aligns perfectly with Kinetic Gas Theory (KGT), which holds that the likelihood of molecular collision P_c can be determined from Refs. [8,40]:

$$P_c = 1 - e^{-\rho V_{rel} A_c \Delta t} \tag{20}$$

where ρ is object spatial density (# per unit volume), V_{rel} is relative velocity in distance per unit time, A_c is the collision cross-sectional area of the object at risk, and Δt is the amount of time the object of interest is transiting the spatial density volume.

As noted in Ref. [8], this expression can be readily simplified by expansion. From Ref. [41],

$$1 - e^{-x} = \frac{x}{1!} - \frac{x^2}{2!} + \frac{x^3}{3!} - \frac{x^4}{4!} + \ldots \tag{21}$$

And for small values of x, the expression for $P_c$becomes:

$$P_c = \rho V_{rel} A_c \Delta t \tag{22}$$

From Ref. [42], the mean time between collisions is found by setting $P_c = 1$:

$$\overline{\Delta t}_{molecular\ collision} = \frac{1}{v_{inertial}\sqrt{2}\,\pi\, d^2 \rho} = \frac{1}{V_{rel} A_c \rho} \tag{23}$$

The formulation in Ref. [35] at first appears different:

$$ACP = F_{r_{min} < r < r_{max}} C_s \tag{24}$$

Where ACP is Annual Collision Probability, $F_{r_{min} < r < r_{max}}$ is the flux of orbiting objects (number of object passages per unit area and year) with sizes in the range of $r_{min} < r < r_{max}$. But defining:

$$F_{r_{min} < r < r_{max}} = \rho V_{rel} \Delta t \tag{25}$$

and

$$C_s = A_c \tag{26}$$

one obtains the same equation as in Refs. [8,39,40].

Key takeaways from this discussion are:

(1) Existing flux and spatial density-based collision likelihood approaches are equivalent;
(2) All of them have A_c in the denominator of the mean time between collisions expression;
(3) If we define the hardbody shape as a sphere, i.e., $A_c = \pi R_E^2$, then these flux or spatial density equations match our assertion that $\left[\frac{\#\ encounters}{time}\right] \propto [R_E^2]$ from above.

This R_E^2 encounter rate relationship works quite well in the LEO regime as was demonstrated in Ref. [39] (Fig. 35).

7.2. Where the encounter rate proportionality to R_E^2 relationship falters

The mean anomaly space can be thought of as a "non-radial" space akin to a unit sphere representation. The linear relationship in mean anomaly space (Fig. 34) is essentially inviolate since the elliptical conjunction area in this space will shrink or expand linearly with R_E.

However, the same cannot be said of the other constituent linear relationship, which is the propensity to admit satellites in neighbouring altitude orbits in the local vertical direction (both up and down) linearly as $R_E$is increased. Fig. 36 shows how the number of RSOs in the vicinity of the Iridium orbital altitude varies as a function of altitude. The horizontal blue bars denote increasing R_E values, which approximately admit neighbouring RSOs in a linear fashion due to the roughly homogenous, stable, relatively high-density LEO regime. In fact, using the PDF of neighbouring RSOs, it is possible to determine how this linear relationship needs to be altered such that when multiplied by the mean anomaly space exponent, encounter rate can properly be mapped by an exponent of R_E as shown in Fig. 37. It can be seen that the exponent ranges from about 1.9 to 2.0 for up to $R_E = 50\ km$.

In stark contrast, a PDF of the GEO regime resembles a "razor edge," whereby spatial density drops away relatively quickly once the selected R_E.value extends away from the populated GEO arc as shown in Fig. 38. This altitude range is driven by the ranges in semi-major axis and eccentricity as was characterized in Fig. 4 of [43]. As was done for the LEO case, we can again determine the density of neighbouring GEO RSOs (Fig. 39) and accompanying R_E exponent (Fig. 40).

Fig. 40 contains a seminal result, in that these exponents allow us to extrapolate GEO encounter rate trends in a justifiable manner, both in the local region (i.e., within 10 km using an average exponent of 1.85) as well as when more than 20 km away (i.e., using an average exponent of 1.2). It's important to remember that these exponential relationships will depend somewhat upon longitudinal and inertial locations throughout the GEO arc as was shown in Fig. 38. Even so, these two "averaged" exponential mapping relations will become important shortly, because they provide us with the ability to "bridge the gap" between collision-relevant research (e.g., Fig. 28) and encounter rate

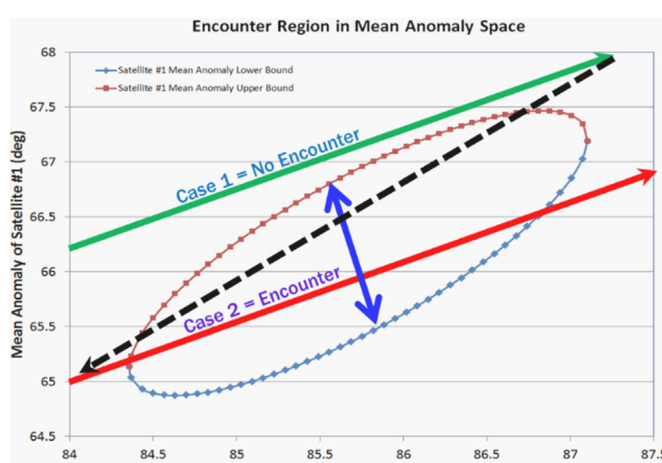

Fig. 34. Encounter geometry in mean anomaly space (representing constituent *likelihood* on a unit sphere).

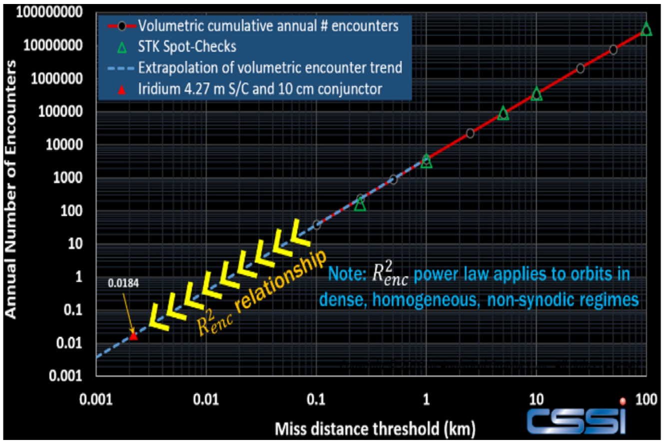

Fig. 35. Demonstration of encounter rate proportionality to R_E^2 using the Iridium constellation (LEO).

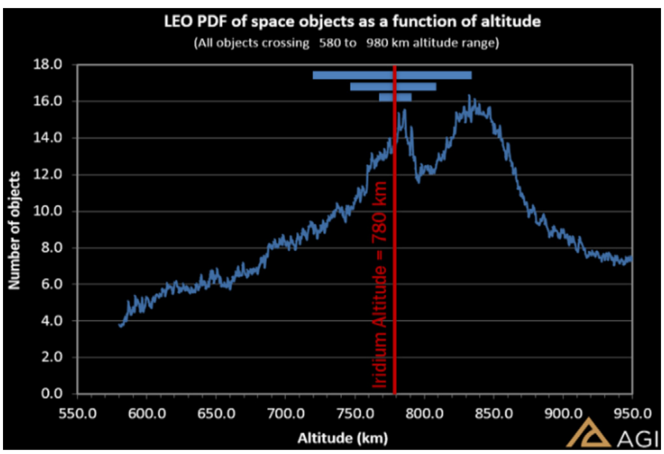

Fig. 36. Comparison of estimated LEO-crossing objects larger than 2 cm vs a 2017 LEO-crossing public catalogue.

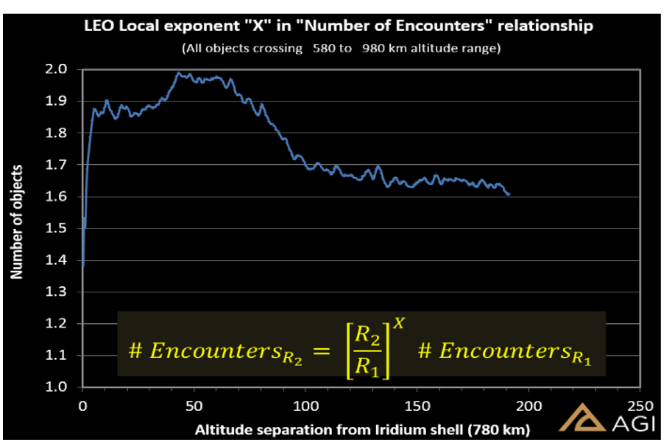

Fig. 37. Combined [altitude + unit sphere] exponent in the neighbourhood of the Iridium constellation.

research (e.g., Fig. 33).

8. Potential pitfalls of using flux-based methods to estimate encounter rates

While using a flux-based Pc assessment approach in LEO should provide a reasonable estimate in a reasonably homogenous environment (i.e. perhaps in the thickest portion of LEO, steering clear of Sun-

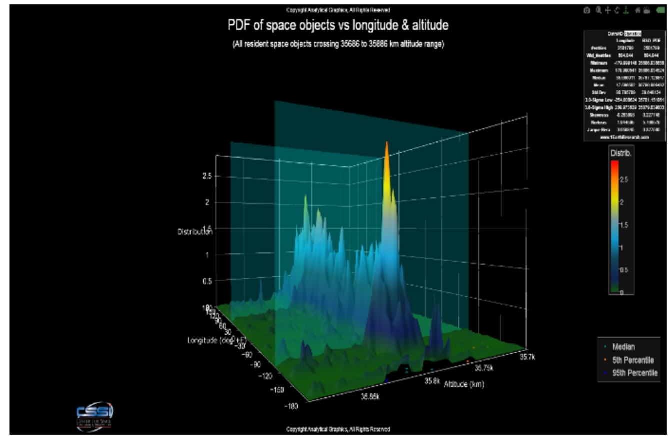

Fig. 38. Probability Density Function of GEO satellites and debris as a function of longitude and altitude.

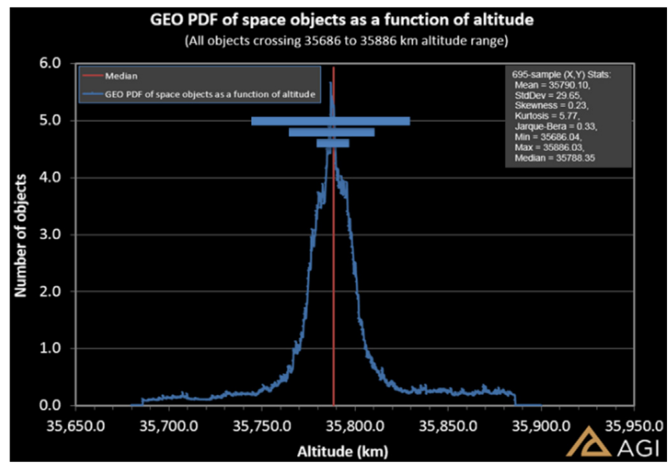

Fig. 39. Longitudinally-averaged Probability Density Function of GEO satellites and debris as f (altitude).

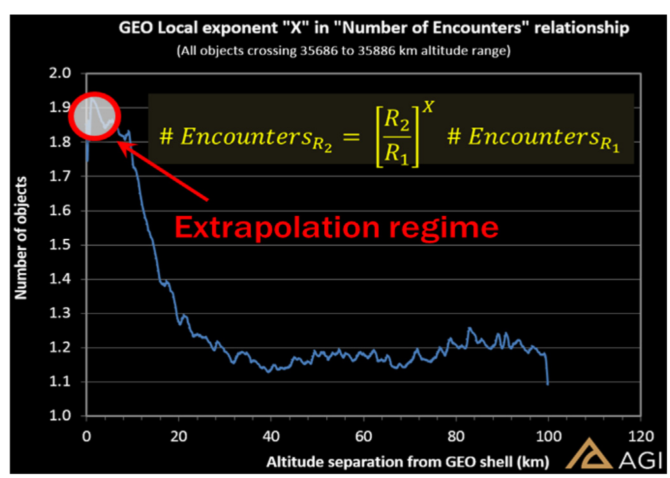

Fig. 40. Combined [altitude + unit sphere] exponent in the neighbourhood of the GEO altitude shell, with an average of 1.85 within 10 km of GEO.

synchronous orbits), the non-homogeneity elsewhere in LEO and in GEO (with synchronicity and an extremely thin operating shell) and sensitivity to binning size may make flux and spatial density assessment approaches unreliable for the following reasons:

(1) GEO flux (spatial density) depictions fail to capture the GEO-

dominating temporal synchronicity, relative motions and interactions of primary and secondary objects in GEO, including gravity well oscillations, etc.
(2) GEO flux is spatially a strong function of both longitude and inertial right ascension, yet there is no way to accommodate this.

Further, it is worth noting that at least three types of spatial density depictions currently exist in space debris and space population models:

- One-dimensional spatial density (i.e. as a function of altitude, Fig. 41) has been used by analysts for many years [44] to attempt to assess collision probability;
- Two-dimensional spatial density (by altitude and latitude, Fig. 42) is currently implemented in both the NASA ORDEM and ESA MASTER models;
- Three-dimensional spatial density (e.g., by altitude, latitude and longitude or inertial right ascension, Fig. 43) as used in AGI's spatial density depictions [45] and the DREAD tool [68,69].

The MASTER and ORDEM models are derived from a combination of historical, empirical (laboratory), simulation and predictive events. In both MASTER and ORDEM, 2D spatial density as a function of altitude and latitude is categorized as a function of debris source/type (explosion fragments, collision fragments, LMRO, NaK droplets, SRM slag, SRM dust, paint flakes, ejecta, and MLI, as well as meteoroids), altitude and latitude. Spatial density, in turn, can be used (and occasionally misused) to derive collision rates.

In the above 1D and 2D functional representations, note that spatial density variations are not accommodated or recognized in either right ascension or longitude. As a 3D spatial density plot readily illustrates (Fig. 43), there is in fact a strong dependency on these "clocking" angles, due to the net perturbative trending (long-duration) that occurs in GEO.

Ultimately, each reduction below three dimensions in the level of spatial density functional dependency (i.e., 2D and 1D) causes more information content to be lost. As is commonly known, such "averaging" can dramatically lower spatial density peaks and raise the spatial density valleys. From the standpoint of trying to assess encounter rates or likelihood of collision, this may be an undesirable consequence.

9. Validity of prorating encounter and/or collision likelihood by active and inactive satellites

In the previous sections, we've characterized collision and encounter rate estimates from external researchers by mapping their results into our desired 167-satellite "normalized" set of satellites. To do this mapping, we've prorated (i.e. scaled) their results by the ratio of active GEO satellites of interest to active GEO satellites those researchers assumed. We further mapped their results by the ratio of GEO debris of interest, to GEO debris analysed by those researchers.

But this mapping approach may not be valid, especially where small GEO sample sizes are concerned. For example, several of the referenced papers [32,34] used GEO active satellite sample sizes of one and twenty three, respectively. While it is gratifying to see that these undersampled results are in family with many other approaches, caution should be exercised when trying to draw conclusions from these results. Another form of undersampling is time-based; for example, while the "AdvCAT evaluation of notional stationkept GEO active satellites" (presented below) uses a reasonably sized set of 167 satellites, the conjunction timespan is undersampled because it only covers 23 days.

We can actually test whether such a prorating technique works by applying it to a large quantity of satellites (i.e., 292 satellites from the eighteen GEO operator set of JSpOC CDMs). Since the 250,495 CDMs for the 167 SDA satellites of immediate interest are embedded within the 292-satellite, 353,170 CDM set, this gives us "ground truth" which can be used to assess prorating technique percent error incurred, as shown in Fig. 44. This figure shows that a 20% error is not uncommon when using this prorating technique. It also shows that the resulting trends (and accuracy of the mapping technique) become more unstable as the sample size shrinks, i.e. is undersampled.

10. Theory and calculation: six internally-developed techniques to estimate GEO collision likelihood and encounter rates

We now introduce six independent approaches and use them to estimate the likelihood of a GEO collision and associated encounter rates. Results from all of these methods are amalgamated into Fig. 59. This methods are:

(1) Statistical evaluation of JSpOC CDMs;
(2) Statistical evaluation of SDC conjunction data;
(3) CSSI's volumetric encounter assessment method;
(4) Statistical evaluation of parametrically-sampled longitudes for notional (simulated) satellites and AdvCAT conjunction analyses;
(5) Statistical AdvCAT evaluation of notional stationkept GEO active satellites
(6) CSSI's simplistic ring assessment

10.1. Method 1: statistical evaluation of JSpOC CDMs

For this first method, we used the same 3.066-year JSpOC 353,170-CDM GEO unique TCA dataset (aggregated over eighteen GEO operators) assessed above to characterize encounter rate variation as a function of miss distance. This can be readily accomplished for any set of operational or simulated conjunction events using a miss distance binning (counting) of the number of unique TCAs (out of the 250,495 CDMs corresponding to the 167 SDA satellites of interest) within each miss distance bin (e.g., Fig. 29). Such binning yields the "green dots" profile shown in Fig. 45. These dots are cumulatively added to obtain the red line shown in Figs. 45 and 46.

Using the newly identified power law relationship for GEO, the empirically-derived red lines can then be extrapolated as shown in Fig. 47. This trend line is also labelled "JSpOC unique conjunctions from CDMs, 2014–2017" in Fig. 59. This extrapolation down to collision-relevant miss distances using an exponent of 1.85 yields an annual likelihood of collision for our chosen 167 SDA satellites of 0.0021 (Fig. 48). Extrapolation to the right uses the precomputed exponent of 1.2.

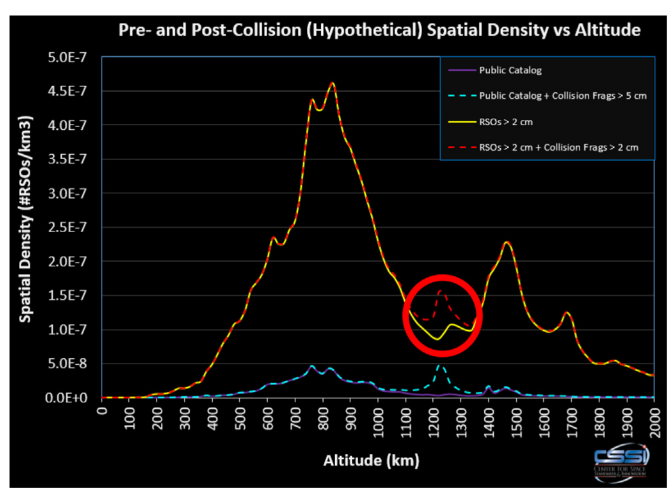

Fig. 41. 1-Dimensional spatial density = f(altitude), showing trends matching the public catalogue, estimated 2 cm catalogue, and a plus-up (red dotted hump at 1200 km) after a hypothetical fragmentation event. (For interpretation of the references to colour in this figure legend, the reader is referred to the Web version of this article.)

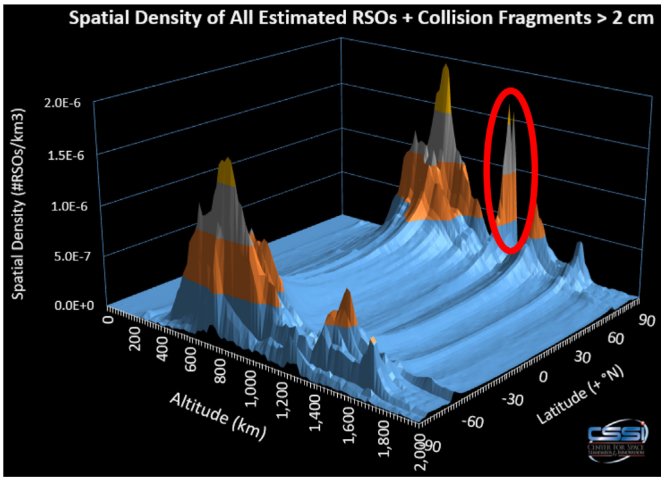

Fig. 42. 2-Dimensional spatial density for the estimated 2 cm catalogue, including the plus-up (red encircled hump at 1200 km) after a hypothetical fragmentation event. Note that this non-latitude-averaged peak is dramatically more pronounced than the 1D depiction indicates. (For interpretation of the references to colour in this figure legend, the reader is referred to the Web version of this article.)

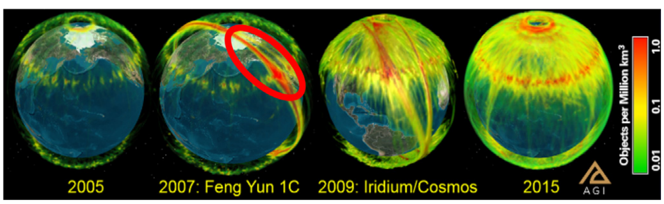

Fig. 43. A sequence of 3-Dimensional spatial density depictions of the public catalogue, including the red-encircled plus-up of the Iridium/Cosmos event. Such a non-longitude-averaged peak is much more pronounced than either 1D or 2D depictions could possibly indicate. (For interpretation of the references to colour in this figure legend, the reader is referred to the Web version of this article.)

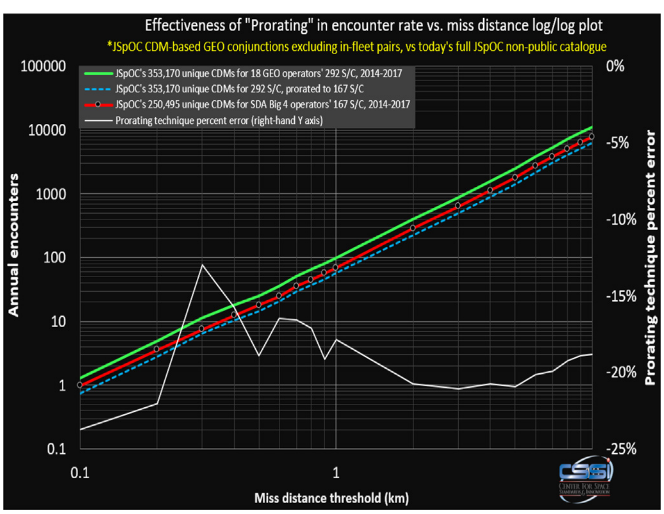

Fig. 44. Effectiveness of "prorating technique" used for mapping disparate collision and encounter rate profiles.

Another interesting conclusion that can be drawn from this JSpOC CDM-based empirical dataset is that the quantity of conjunction alarms generated also follows that same power law (i.e., with exponent ≈ 1.85).

Accounting for unmodelled manoeuvre effects, cross-tagging,

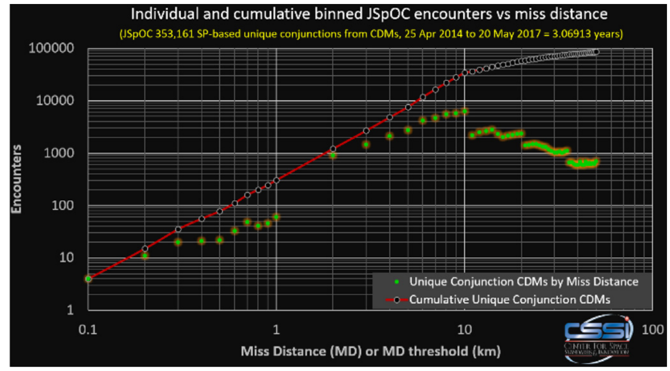

Fig. 45. Assembly of JSpOC CDM-based "cumulative annual GEO unique encounters" trend in log/log space.

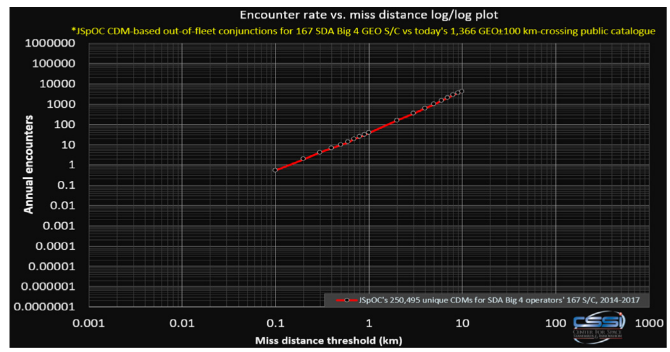

Fig. 46. Assembly of JSpOC CDM-based "cumulative annual GEO unique encounters" trend in log/log space.

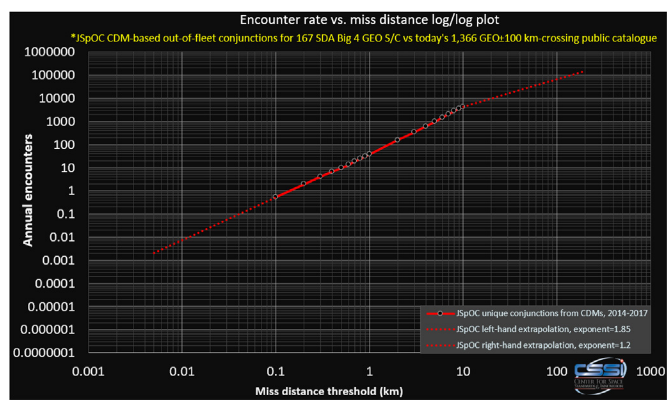

Fig. 47. Left- and right-hand extrapolation of 167 satellite trend using pre-computed power law exponents 1.85 & 1.2.

operator range transponder biases of up to 15 km, a potential lack of sensor and observing site diversity and lagging orbit determination updates and uploads, current systems typically face total relative primary-to-secondary uncertainties of 10 km or more. In order to protect one's spacecraft from such errors, this should require satellite operators to manoeuvre whenever the miss distance at TCA is less than (10 km + some margin). This FDS conjunction processing and manoeuvre rate is denoted by the red circle superimposed on the JSpOC red trend line shown in Fig. 49, indicating thousands of conjunction events must be evaluated by FDS with 4,203 manoeuvres annually.

In stark contrast, one can envision a system that ingests much larger quantities of diverse observational data, relies on a much more diverse set of observing sites and sensors, incorporates participating operator manoeuvre plans and solves non-cooperatively for any others, generates realistic covariances and operates on a more responsive orbit

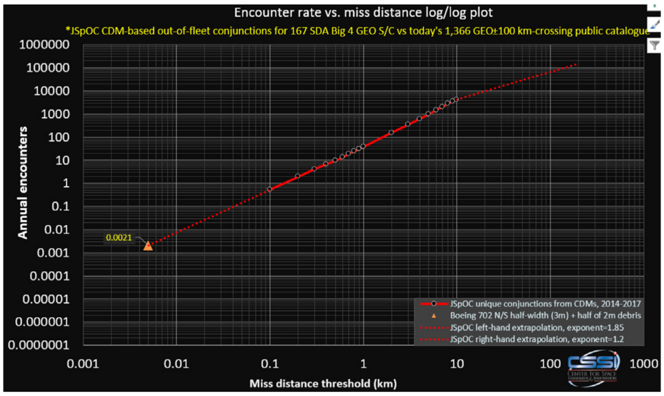

Fig. 48. Extrapolation of encounter rate trends permits estimation of hardbody collision likelihood (0.0012 annually for these 167 satellites).

determination, processing and distribution timeline. In this case, it should be possible to reduce the relative positional errors for each conjunction pair down to around 500 m. This dramatically reduces the number of identified collision threats from 4203 to only ten. The remaining 99.8% of the identified collision threats from the 10 km conjunction assessment system are false alarms.

One such futuristic SSA system is AGI's Commercial Space Operations Center, or ComSpOC. ComSpOC [45–48] is fully operational today, providing satellite operators with timely, actionable and decision-quality SSA data for their avoidance manoeuvre planning process, thereby separating serious collision events from numerous false alarms (see Fig. 49).

10.2. Method 2: statistical evaluation of SDC conjunction data spanning 2014–2017

The Space Data Centre (operated by Analytical Graphics for the Space Data Association) [49] houses historical Space Data Center (SDC 1.0) conjunction results. In operation since 15 July 2010, the SDC now performs conjunction assessments for 34 participating operators. We selected SDC 1.0 conjunction data from the 3.229-year time span of 10 June 2014 to 1 September 2017 containing 53,909 unique conjunction events. Aggregating these conjunction results yields a similar curve in log/log space ("SDC unique conjunctions, 2014–2017" in Fig. 59).

One can observe that the SDC 1.0 encounter rate line is 29% lower than the JSpOC CDM line at the 10 km miss distance, rising to 44% lower at 1 km. Additionally, the SDC 1.0 trend line varies more from the "log-linear" trend above 1 km. Likely causes for this artefacts are:

(1) The SDA operators rely on SDC conjunction reports to identify collision risks and pre-emptively avoid them. In so doing, the amount of close conjunctions are reduced in the SDC dataset.
(2) SDC 1.0 conjunction screening uses the publicly disclosed TLEs and SP ephemerides to assess conjunctions, whereas the JSpOC CDM product includes non-public items. From above, this factor (i.e., $1.52 < SF_{T2C} < 1.96$) can introduce more conjunctions into the JSpOC CDM dataset.
(3) The JSpOC results have not incorporated planned manoeuvres, and even when they do for some operators, other operators' planned manoeuvres are not foreseen. For that reason, conjunctions can often be introduced which are not really present, e.g., if the satellite performs its E/W and N/S manoeuvres to stay inside of its allocated stationkeeping box as planned, averting collision risk with other active satellites in their stationkeeping boxes.

10.3. Method 3: encounter volumetric assessment

A volumetric approach [37,38] was developed as a planning and characterization tool to estimate the possibility and frequency of satellite encounters with other satellites and debris objects for a prospective orbit regime. The encounter volume is defined by an ellipsoid that is constant in size, shape, and orientation in the satellite's Radial-In track-Cross track (RIC) frame and is used to rapidly estimate the average rate of encounters one can expect as a function of orbital regime, catalogue size, and encounter radius. This is used to estimate the number of times a circular equatorial satellite at geosynchronous altitude will encounter objects from a space object catalogue. STK/AdvCAT was used to independently confirm estimates generated using this technique.

This method was used to estimate the annual number of encounters between SDA Big 4167 actives and the public catalogue dated 17 November 2016 ("Volumetric method" in Fig. 59).

10.4. Method 4: 0.1° longitude parametric AdvCAT sampling

In this method, all possible 0.1° longitudinal stationkeeping boxes were sampled by introducing a fictional satellite at the centre of each box (e.g., 179.95° W, −179.85° W, …, 179.95° E) and using System Tool Kit's Advanced Conjunction Assessment Tool (AdvCAT) function to assess the annual number of conjunctions observed as a function of longitude and screening radius ranging from 1 km to 200 km. This analysis was performed by holding all 3600 fictional satellites in the centre of their respective boxes (i.e., Keplerian motion with no drift allowed). All 435 active GSO satellites were then removed from the public TLE catalogue of 17 Nov 2016, and the remaining objects propagated for 18 months to reflect a full drift cycle about the gravity wells. Screening was conducted for the period from 4 Dec 2016 to 4 June 2018. The raw results are shown in Fig. 50. These trends show a strong dependence with proximity to the GEO gravity wells (Fig. 51) and match very well quantitatively with those of [18] and qualitatively with those of Fig. 3 in Ref. [50]. As well, the ratios evident in the raw 100 km line (Fig. 52) match well with the "factor of seven" increase between gravity well risk and away from gravity wells, discovered by McKnight [8]. Applying a 3° longitudinal moving average filter to the raw data of Fig. 50 yields Fig. 53.

To estimate encounter and collision rates using this technique, each of the filtered trend lines in Fig. 53 were evaluated at the longitudes occupied by each of the SDA Big 4's 167 satellites, and then the number of annual encounters was aggregated across those 167 satellites to produce the desired encounter rate trend line ("AdvCAT Parametric Longitudinal Sampling" in Fig. 59).

10.5. Method 5: stationkeeping box cycle emulation

This method again uses AGI's AdvCAT module to detect conjunctions. But in this method, TLEs for the 167 SDA satellites are specifically

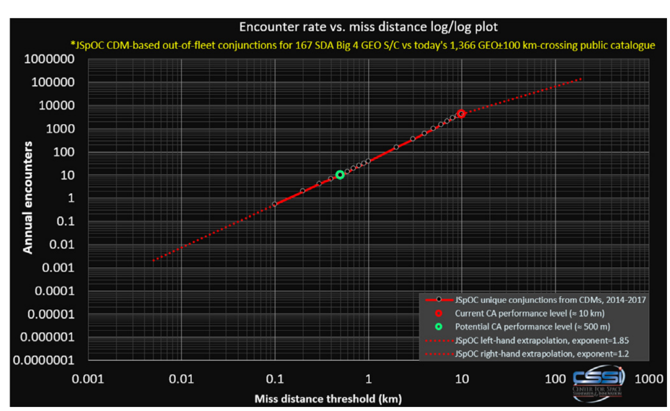

Fig. 49. Comparison of number of encounters at current and potential CA quality levels.

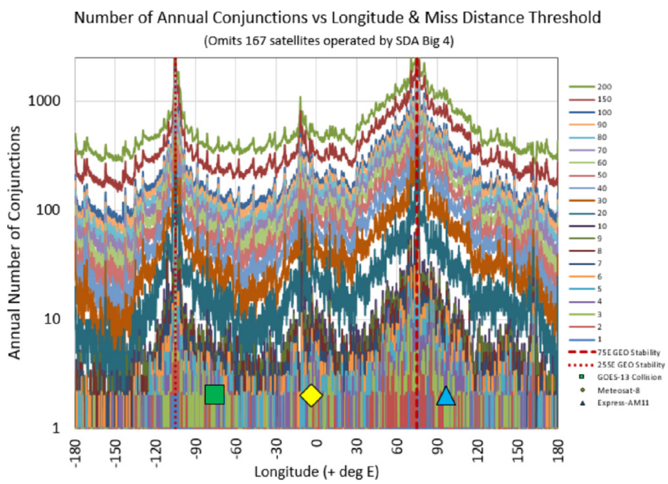

Fig. 50. AdvCAT parametric assessment of annual conjunctions vs longitude and miss distance threshold for Eutelsat, Inmarsat, Intelsat and SES′ 167 spacecraft.

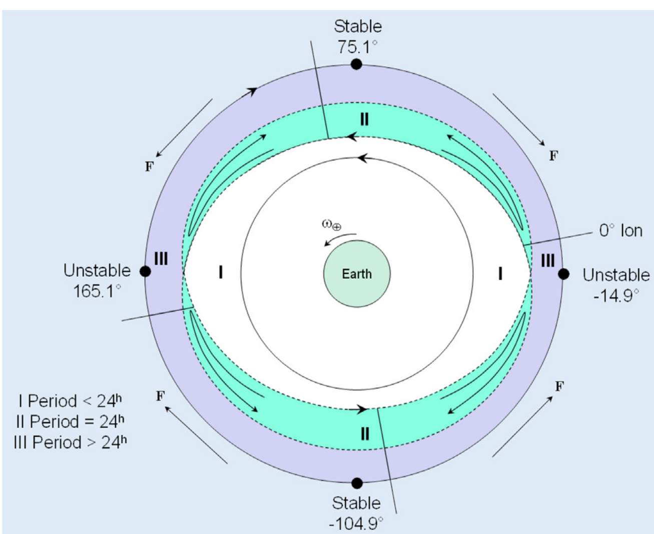

Fig. 51. Gravity well positions for GEO debris.

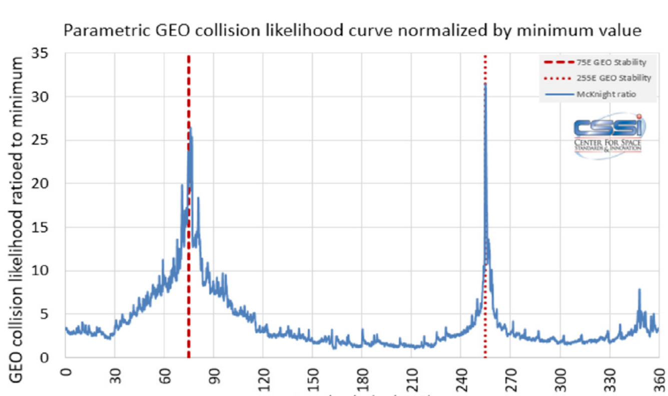

Fig. 52. AdvCAT parametric collision likelihood assessment height is similar to SwissRE flux-based approach, but peak-to-valley ratio of over thirty is much larger than the factor of seven originally noted in Ref. [8].

constructed such that each satellite is placed at its starting extent of its stationkeeping cycle and "flown" thru the cycle for a period of 23 days. The longitudinal placement of these 167 satellites is as shown in

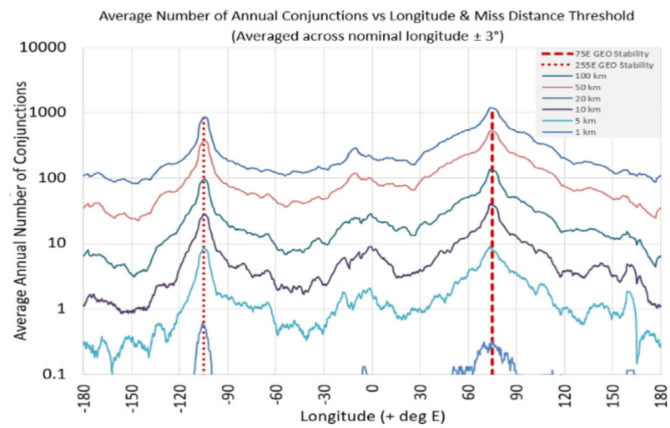

Fig. 53. Moving average filtered AdvCAT parametric assessment of annual conjunctions vs longitude and miss distance threshold for Eutelsat, Inmarsat, Intelsat and SES′ 167 spacecraft.

Fig. 54, where the Earth's gravitational GEO resonance-induced rate-of-change for semi-major axis is also depicted.

The 23-day AdvCAT analysis timespan was selected from Fig. 57 as the typical minimum stationkeeping cycle duration. This allows a majority of satellites to fly thru the full extent of their stationkeeping box occupancy, while keeping the satellites within their box. But we caution that this 23-day timespan may likely under-sample the resulting encounter rate statistics.

Against these 167 specially-constructed TLEs, a TLE catalogue from 1 October 2015 was assessed for conjunctions using AdvCAT over a 23-day timespan. The resulting cumulative trend of the number of encounters as a function of miss distance ("AdvCAT stationkept unique conjunctions" in Fig. 59) was obtained by upscaling AdvCAT results via:

$$\frac{\#Enc_{\text{Stationkept}}}{yr} = \left[\frac{AdvCAT_{23\ day}}{23\ days}\right]\left[\frac{365.25\ \text{day}}{1\ yr}\right] \tag{27}$$

10.5.1. Suitability of SDP4 propagator for modelling of the GEO stationkeeping cycle

We first confirmed that the SGP4 semi-analytic propagator does include the requisite C_{22}/S_{22} (tesseral) gravity resonance effects [51] necessary to adequately model east/west perturbations. Using SGP4 to propagate the specially constructed TLEs for the GEO active satellites produced longitudinal motion as anticipated (Fig. 55 and Fig. 56).

10.6. Method 6: simplistic ring assessment method

The ring approach is somewhat similar to the volumetric approach.

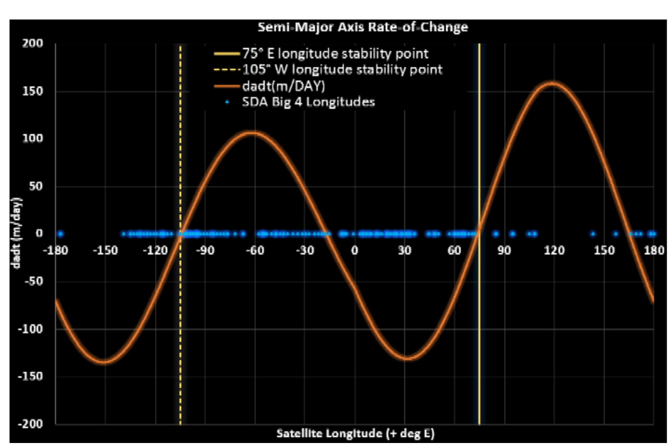

Fig. 54. Longitudinal spread and semi-major axis rate of SDA 167 satellites.

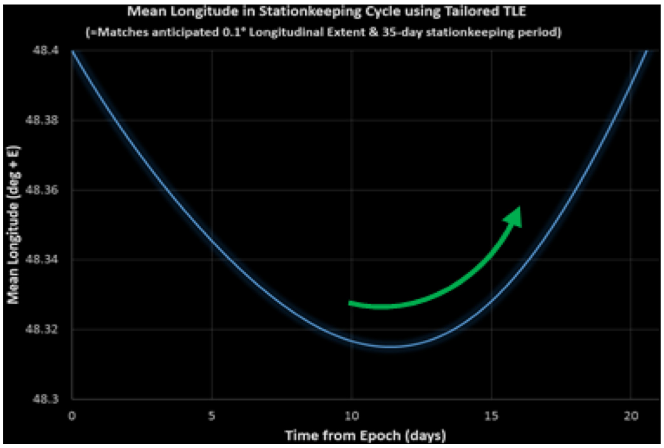

Fig. 55. Progression of mean longitude at 48.35° E.

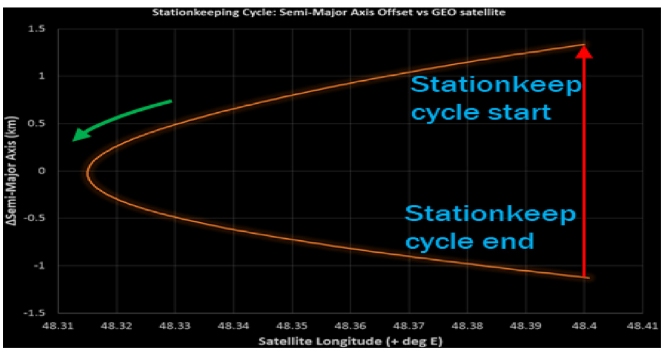

Fig. 56. Progression of semi-major axis at 48.35° E.

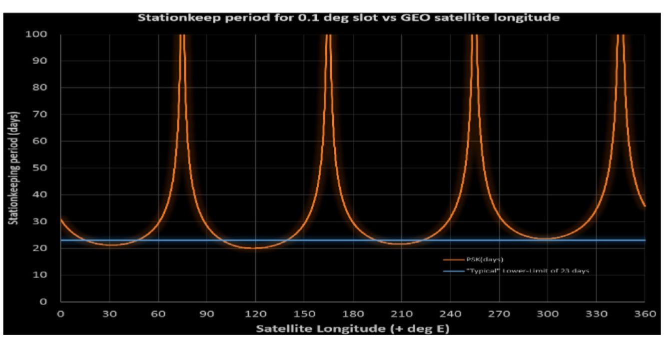

Fig. 57. Typical stationkeeping period vs longitude.

An equatorial ring is created at geosynchronous circular orbit altitude with a prescribed width (Fig. 58). A count is performed of all the times in a year that space catalogue objects pass through the ring. Assuming uniform random spacing of the GEO active satellite along the ring, the probability that an active satellite would be at the specific debris crossing spot on the ring when a single debris object crosses the ring is simply defined as:

$$\frac{\#Enc_{\text{ring}}}{yr} = \left[\frac{\#revs_{debris}}{1\ day}\right]\left[\frac{365.25\ \text{day}}{1\ yr}\right] \times \left[\frac{\text{size}_{active\ \ radial}}{width_{ring}}\right]\left[\frac{\text{size}_{active\ \ intrack}}{2\pi r_{ring}}\right] \tag{28}$$

Where $\text{size}_{active\ \ radial}$ is the dimension of the active spacecraft along the radial dimension (e.g. 6 m), $\text{size}_{active\ \ intrack}$ is the in-track active satellite dimension, $width_{ring}$ is the width of the ring being analysed (e.g. 10 km), and r_{ring} is the radius of the ring (e.g., 42164.172 km).

As with the volumetric approach, STK/AdvCAT was used to independently check this technique.

Application of the ring method using a GEO ± 10 km planar ring and TLE catalogue from 17 November 2016 yields the "AGI simplistic ring method" point in Fig. 59.

11. Surveys & anecdotal accounts of suspected collisions

Collisions in GEO are quite infrequent, and even if one knew precisely which few GEO collisions have occurred, it would be academically impossible to draw a statistically significant likelihood of collision conclusion from such an undersampled dataset. Nevertheless, it's likely that unverified indications of GEO collisions have occurred:

- GOES-13–22 May 2013 at λ = 74.6° W [52]
  - Micrometeoroid or space debris hit solar array arm [53].
  - Returned to normal operations on 6 June 2013
- MeteoSat8 - 22 May 2007 at λ = 3.5° E [54].
  - Damage sustained in a radial thruster pair
  - Hypothesis: micro-meteorite or space debris collision
  - Redundant systems, able to serve as in-orbit backup
- Express-AM11–28 March 2006 at λ = 96.5° E [55].
  - "Failed due to sudden external impact"
  - "The cause most probably was space garbage of unknown origin"
  - Sufficiently intact to send it into a graveyard orbit
- In a recent technical exchange between GEO spacecraft operators, an operator acknowledged that one of their satellites had a collision with a small fragment (either micrometeoroid or debris) in the last ten years, even though the event was not publicly announced.
- There are indications of many other GEO satellite failures and breakup events as shown in Table 1.

Some wonder how it could be possible that a GEO collision would not be announced and/or acknowledged by a satellite operator. Would we not know if and when a GEO collision has occurred, since operators routinely and transparently share such collision/anomaly info? The reality is that many practical things could prevent transparency regarding a potential collision event in any orbit regime, to include implications to satellite insurance rates, stock holder and/or investor concerns, political considerations, cultural inhibitions, customer confidence, and commercial services competition.

12. Overall GEO active satellite collision likelihood

Overlaying CSSI methods 1–6 yields Fig. 59. Extrapolating CSSI methods 1–5 to hardbody collision relevance (again using an exponent of 1.85) and adding all identified relevant external research yields Fig. 60, providing a coherent assessment of collision likelihood and encounter rate trend lines for 167 SDA satellites against the current public RSO catalogue.

Combining our estimates of the space population (Fig. 3) with scale

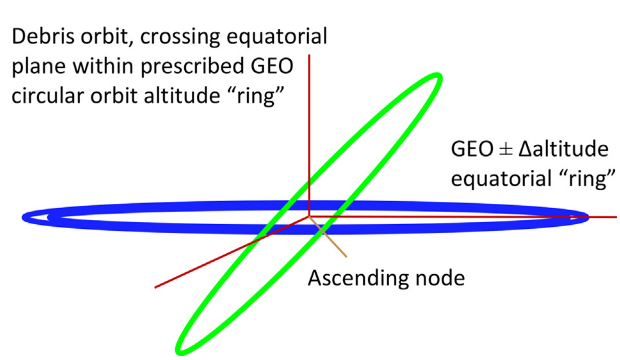

Fig. 58. "Ring" method determines collision likelihood from all catalogue orbits crossing an equatorial GEO ± 10 km planar ring.

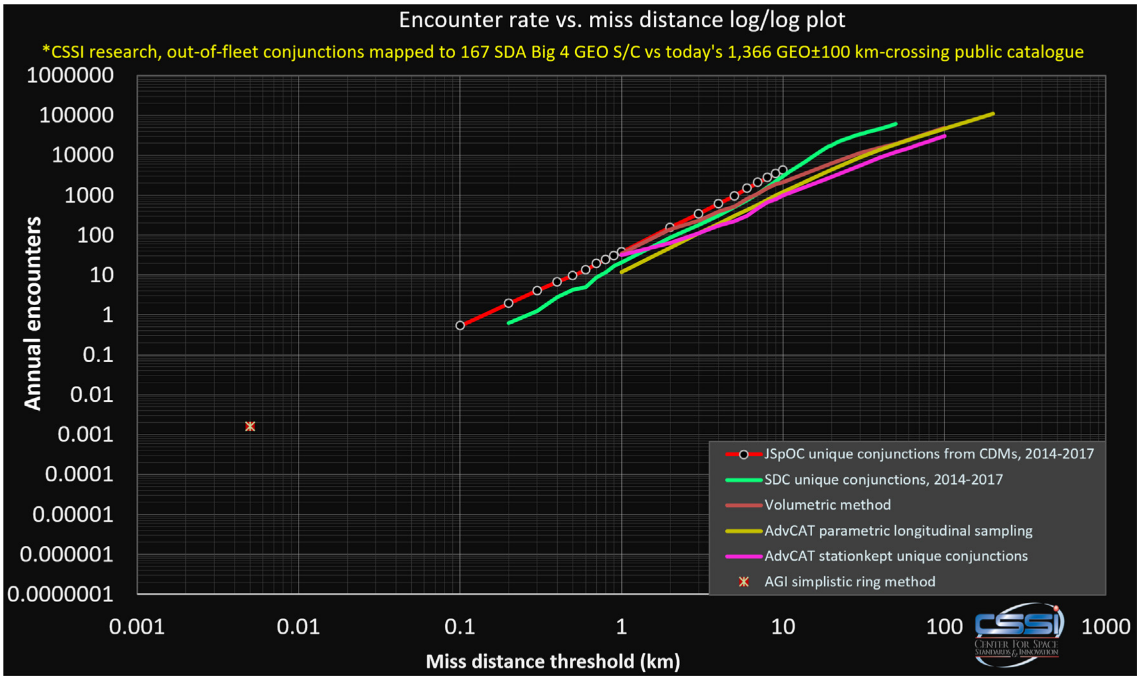

Fig. 59. Six CSSI GEO collision and/or encounter rate profiling techniques for 167 SDA Big 4 operator satellites.

factors SF_{T2C} or $SF_{T2C\ active}$estimated previously, the 167-satellite encounter rate estimates can be approximately mapped to other conditions, where $\mathcal{L}_{167\ 5m\ public}$ is the likelihood of collision (for all collision-relevant results) for 167 satellites versus a 2017 RSO public catalogue at our assumed collision-inducing miss distance of 5 m (drawn from Fig. 60):

(1) All public 478 actives GEO ± 100 km satellites vs public catalogue (Fig. 61);

$$\mathcal{L}_{478\ vs\ public} = \left[\frac{478_{public}}{167_{SDA}}\right]_{actives} \mathcal{L}_{167\ 5m\ public} \tag{29}$$

(2) All active GEOs vs all tracked RSOs (Fig. 63);

$$\mathcal{L}_{All\ trkd} = SF_{T2C}\left[\frac{478_{public}}{167_{SDA}}\right]_{actives} \mathcal{L}_{167\ 5m\ public} \tag{30}$$

(3) All active GEOs vs all 1912 RSOs estimated to be larger than 20 cm (Fig. 65);

$$\mathcal{L}_{20\ cm} = \left[\frac{SF_{T2C} active\ \ 478_{public}}{167_{SDA}}\right]_{actives} \times \left[\frac{1912_{20\ cm}}{1366_{public}}\right]_{inactives} \mathcal{L}_{167\ 5m\ public} \tag{31}$$

(4) All active GEOs vs all 33,293 RSOs estimated to be larger than 1 cm (Fig. 67);

$$\mathcal{L}_{1\ cm} = \left[\frac{SF_{T2C} active\ \ 478_{public}}{167_{SDA}}\right]_{actives} \times \left[\frac{33,\ 293_{1\ cm}}{1366_{public}}\right]_{inactives} \mathcal{L}_{167\ 5m\ public} \tag{32}$$

Figs. 61, 63, 65 and 67 show the resulting mapped encounter rate log/log trends using the above mapping relationships.

Based upon observed relative velocities ranging from nearly zero up to 4 km/s, coupled with breakup modeling incorporating low-velocity accommodations, we identified debris larger than 20 cm as being potentially capable of generating tertiary debris fragments sufficiently large to spawn follow-on (cascading) collisions. This was the motivation for Case (3) above, "All active GEOs vs all RSOs > 20 cm" case (Fig. 65).

It has long been held that hypervelocity collisions with 1 cm and larger debris fragments can terminate a satellite mission. While we have shown above that GEO collisions are typically not hypervelocity situations, we also found that in certain conditions GEO collision relative velocities can be as high as 4 km/s. Because these cases are approaching hypervelocity conditions and because mission susceptibility assessments are highly variable and imprecise, it may be advisable to examine the likelihood of collision against 1 cm objects as a conservative limit for GEO as shown in Case (4), "All active GEOs vs all RSOs > 1 cm" (Fig. 67).

Multiplying these resulting averaged annual likelihoods of GEO collision at 5 m miss distance by $SF_{Off-[N/S]}$ and inverting yields the average time between collisions (in years) as estimated using each method portrayed Fig. 62, Fig. 64, Fig. 66 and Fig. 68.

The above estimates have been extensively averaged, both in time, longitude and inertial right ascension dimensions. Our results (Fig. 52) confirm those of McKnight [8] which indicate that the likelihood of collision near the gravity wells is as much as seven times larger than away from them. In fact, we can now multiply the median $\mathcal{L}_{167\ vs\ public}$ value of the eight clustered collision likelihood results of Figs. 60 and 61, Figs. 63, Figs. 65 and 67 by the profile contained in Fig. 53 normalized to an average value of 1.0 by the summation of profile heights extant at each of the 167 SDA satellite longitudes, obtaining Fig. 69.

13. Collision risk = Likelihood * Consequence

This paper so far has been solely focused on assessing the average likelihood that an active GEO satellite will generically "encounter" (or specifically collide with, if the encounter screening radius matches the combined hardbody radii of the conjuncting objects) another GEO object. So far we have steadfastly referred to the likelihood of a collision (rather than "collision risk"). But ideally we would also like to assess collision risk, where:

$$Risk = Likelihood\ \times Consequence \tag{33}$$

Likelihood of a collision occurrence is a straightforward concept to grasp with little room for disagreement. Collision consequence,

Table 1
GEO-proximity satellite failures and breakups, 1977 to 2013.

Common Name	SSC	Ref	Int'l Desig.	Event Date	Hp (km)	Ha (km)	Cat/Assess	Current status
Cosmos 862	9495	[56]	1976-105A	15 May 1977	4089	36389	1	breakup
Cosmos 931	10150	[56]	1977-068A	24 Oct 1977	5858	34489	1	breakup
Cosmos 903	9911	[56]	1977-027A	08 Jun 1978	1325	39035	2	no longer on orbit
Ekran 2	10365	[57]	1977-092A	23 Jun 1978	35785	35800	1	breakup
Cosmos 1030	11015	[56]	1978-083A	10 Oct 1978	685	39760	4	no longer on orbit
Cosmos 1030	39447	[56]	1978-083T	10 Oct 1978	4849	35545	1	breakup
Cosmos 917	10059	[58]	1977-047A	30 Mar 1979	2775	37586	2	breakup
Cosmos 917	26964	[56]	1977-047E	30 Mar 1979	4128	35886	1	breakup
Cosmos 917	27883	[56]	1977-047F	30 Mar 1979	3716	36389	1	breakup
Cosmos 917	27884	[56]	1977-047G	30 Mar 1979	3603	36584	1	breakup
Cosmos 1124	11509	[58]	1979-077A	09 Sep 1979	2627	37851	1	breakup
Cosmos 1124	32982	[56]	1979-077H	09 Sep 1979	2627	37851	6	breakup
Cosmos 1109	11417	[56]	1979-058A	Mid-Feb 80	3804	36675	1	breakup
Cosmos 1261	12894	[56]	1981-031G	Apr/May 81	6039	34347	1	breakup
Cosmos 1191	11871	[56]	1980-057A	14 May 1981	5006	35472	1	breakup
Cosmos 1191	27897	[56]	1980-057K	14 May 1981	3976	36646	1	breakup
Cosmos 1247	12303	[58]	1981-016A	7 Oct 1981	4285	35753	4	breakup
Cosmos 1247	26786	[56]	1981-016J	20 Oct 1981	4815	34758	1	breakup
Cosmos 1247	28270	[56]	1981-016L	20 Oct 1981	4589	35888	1	breakup
Cosmos 1285	12627	[58]	1981-071A	21 Nov 1981	6037	34778	4	breakup
Cosmos 1285	13961	[56]	1981-071F	21 Nov 1981	6037	34778	1	breakup
Cosmos 1261	12376	[58]	1981-031A	12 May 1982	5795	34546	3	breakup
DSP 5 (Ops-3165)	8482	[59]	1975-118A	16 Dec 1982	35,593	35,881	1	unknown failure
Cosmos 1481	14192	[56]	1983-070E	09 Jul 1983	2064	37863	1	breakup
Cosmos 1481	20412	[56]	1983-070F	09 Jul 1983	2980	36739	1	breakup
Cosmos 1456	14301	[56]	1983-038H	13 Aug 1983	730	39630	4	no longer on orbit
Cosmos 1317	35512	[56]	1981-108 M	Late-Jan 84	1315	39055	1	breakup
Cosmos 1317	14736	[56]	1981-108G	Late-Jan 84	8181	32297	1	breakup
Cosmos 1278	12547	[56]	1981-058A	Early-Dec 86	2665	37690	2	no longer on orbit
OV2-5 R/B	3432	[57]	1968-081E	21 Feb 1992	35436	36303	1	breakup
Telstar 401	22927	[59]	1993-077A	11 Jan 1997	35773	35814	1	abrupt TT&C failure
Kupon	25045	[59]	1997-070A	01 Mar 1998	35752	35813	1	stabiliser failed
Cosmos 2350	25315	[59]	1998-025A	01 Jul 1998	35788	35805	1	seal failure
Solidaridad 1	22911	[59]	1993-073A	27 Aug 2000	35772	35817	1	SCP failure (primary & backup)
STRV 1c	26610	[59]	2000-072C	16 Nov 2000	711	39767	1	design flaw
STRV 1d	26611	[59]	2000-072D	16 Nov 2000	628	39263	1	design flaw
Cosmos 2397	27775	[59]	2003-015A	01 Jun 2003	35550	35919	1	fuel tank press. system gas leak
Telstar 4	23670	[59]	1995-049A	19 Sep 2003	35777	35825	1	primary power bus short circuit
AO-40 (Phase 3D)	26609	[59]	2000-072B	01 Jan 2005	1060	58774	1	plugged valve vent
Intelsat 804	25110	[59]	1997-083A	14 Jan 2005	35766	35824	1	sudden EPS anomaly
Express-AM11	28234	[60]	2004-015A	28 Mar 2006	36050	36122	1	impact attributed to space debris
SinoSat 2	29516	[59]	2006-048A	01 Oct 2006	37814	38188	1	failed solar array/ant. deploy
Beidou 2A	30323	[57]	2007-003A	02 Feb 2007	195	41775	70–100	breakup
MeteoSat8	27509	[59]	2002-040B	22 May 2007	35789	35793	1	collision w/micrometeorite/debris
Eutelsat W2M	33460	[59]	2008-065B	28 Jan 2008	35785	35800	1	major power system anomaly
Amazonas 1	28393	[59]	2004-031A	01 May 2008	35849	35890	1	defective pyrovalve
EchoStar II	24313	[59]	1996-055A	14 Jul 2008	35763	35803	1	unknown failure
DSP 23 (USA 197)	32287	[59]	2007-054A	mid-Sep 2008	35752	35773	1	unknown failure
KazSat 1	29230	[59]	2006-022A	01 Nov 2008	36072	36100	1	computer glitch
NigComSat 1	31395	[59]	2007-018A	01 Nov 2008	35804	35813	1	power supply failure
CHINASAT 6A	37150	[59]	2010-042A	04 Sep 2010	35789	35796	1	helium leak
Briz-M Stage	34711	[57]	2009-016B	13 Oct 2010	3766	33379	1	breakup
Briz-M Stage	38247	[57]	2012-016C	13 Oct 2010	3147	34057	1	breakup
Briz-M Stage	40385	[57]	2015-005B	13 Oct 2010	3277	62734	1	breakup
Eutelsat W3B	37206	[59]	2010-056A	28 Oct 2010	267	33350	1	propulsion system anomaly
CZ-3C Third Stage	37211	[57]	2010-057B	01 Nov 2010	160	35780	50 +	breakup
CZ-3B Third Stage	38015	[57]	2011-077B	21 Dec 2011	230	41715	60 +	breakup
GOES-13	29155	[56]	20006-018A	22 May 2013	35771	35818	1	Micrometeoroid likely hit
Ekspress-MD1	33596	[59]	2009-007B	04 Jul 2013	36074	36171	1	faulty orientation

however, is open to interpretation. The following are some typical collision consequences one might adopt:

(a) A collision between one or more massive objects which renders the operator's mission orbit unusable (due to the large quantity of fragments posing high secondary collision likelihood with the operator's remaining orbit constellation);
(b) A collision between one or more massive objects which renders the operator's mission orbit operationally untenable (i.e., too operationally challenging to manage, due to the high analytical and Space Situational Awareness costs of identifying collision risks and repeatedly manoeuvring to avoid them);
(c) A collision with a mission-critical satellite which renders it ineffective or dead, causing the mission to be degraded or fail.

All of the above definitions of "consequence" are appropriate and legitimate, depending upon the circumstances. But for the purpose of illustration here, the first definition (generation of many debris fragments, e.g., > 10 fragments) is adopted.

But how does one know how many fragments will be generated? Explosion and collision events cause fragments to be ejected at velocities up to a few kilometres per second in extreme cases. But unlike

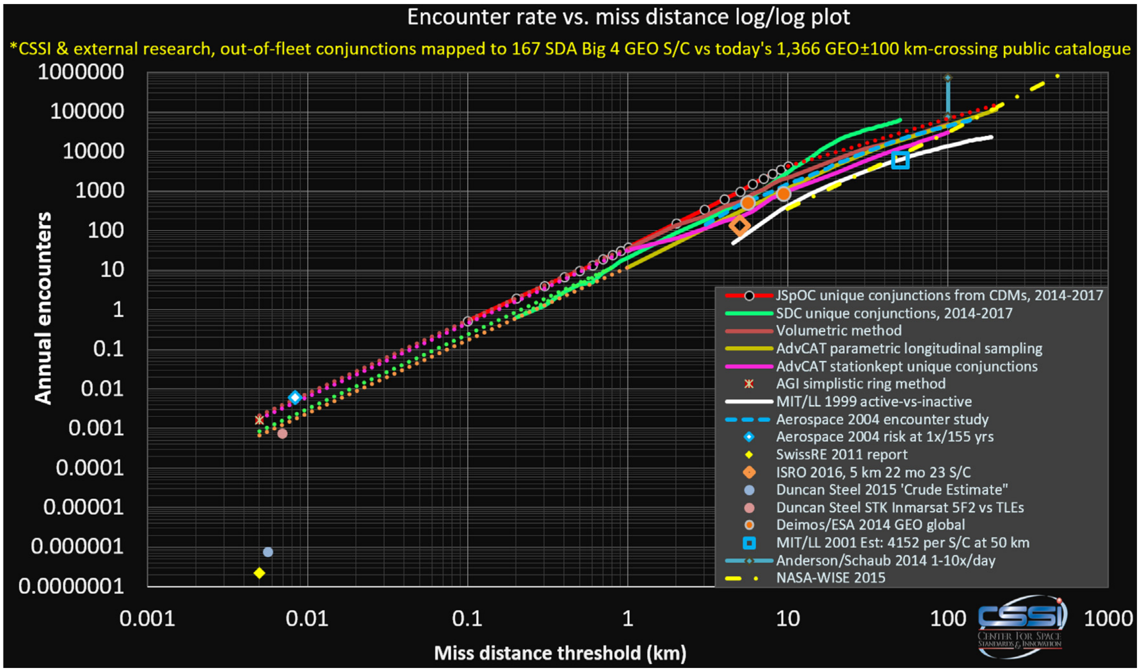

Fig. 60. Comparison of external and CSSI results for 167 SDA Big 4 operator satellites, including extrapolation via miss distance ratio power law (exponent = 1.85 below 1 km and 1.2 above 10 km).

almost all LEO collisions, GEO relative collision velocities are well below "hypervelocity impact" conditions. As shown in Fig. 16, a GEO conjunction relative velocity of 796 m/s is commonly observed corresponding to the conjunction of equatorial with 15°-inclined debris. Other relative velocities of 1450 m/s can be observed extending up to, most likely stemming from the conjunction of geosynchronous transfer orbit (GTO).

The often-cited 40 J/g catastrophic threshold of Energy-to-Mass Ratio (EMR, in Joules of impactor energy divided by mass of the target in grams) commonly used in low-fidelity hypervelocity fragmentation estimator models [61] is not a precise breakpoint between catastrophic and non-catastrophic collisions. McKnight [62] suggests instead adopting > 35 J/g for complete catastrophic collision where fragments' mass distribution follows a power law, a "transition zone" of 15–35 J/g for complete breakup where fragments' mass distribution follows an exponential curve, and < 15 J/gm for "disruption."

A fragmentation event stemming from a non-hypervelocity collision is further complicated by the "plastic deformation" of the colliding materials. McKnight [62] states that "*at relative velocities below the speed of sound in the material (i.e., 6 km/s for aluminium and steel), resultant breakup effects can range from rigid body dynamics, to simple elastic deformation to plastic waves (complex deformation, tears and some*

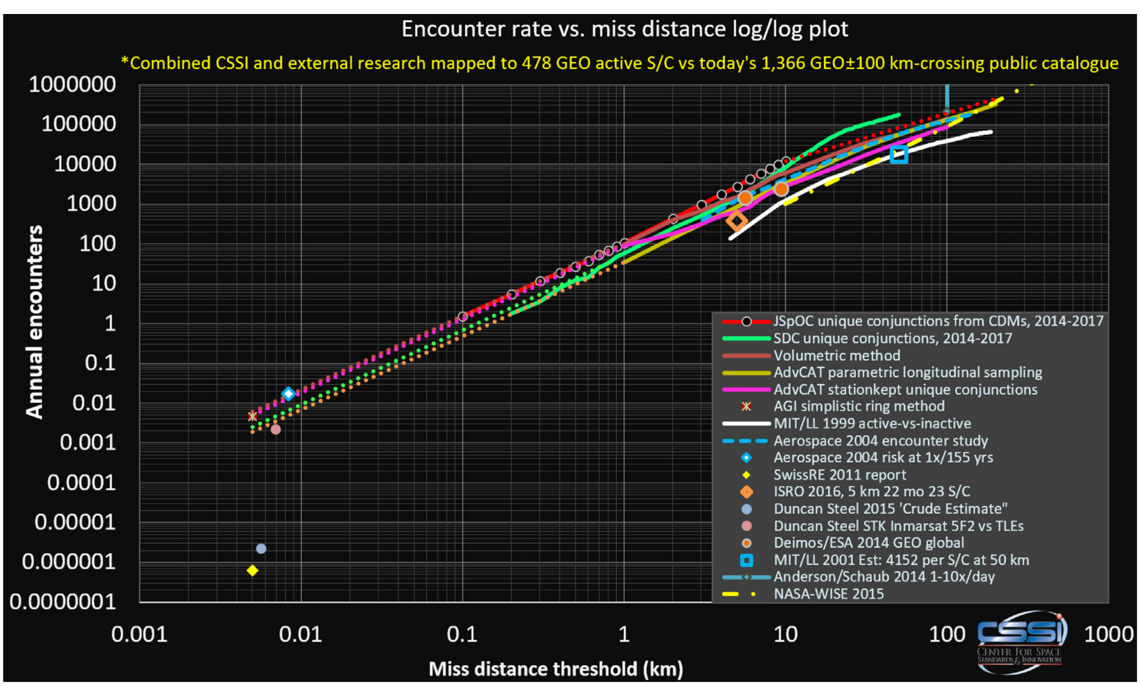

Fig. 61. Estimated GEO encounter rates for 478 active GEO ± 100 km satellites versus the 2017 RSO public catalogue.

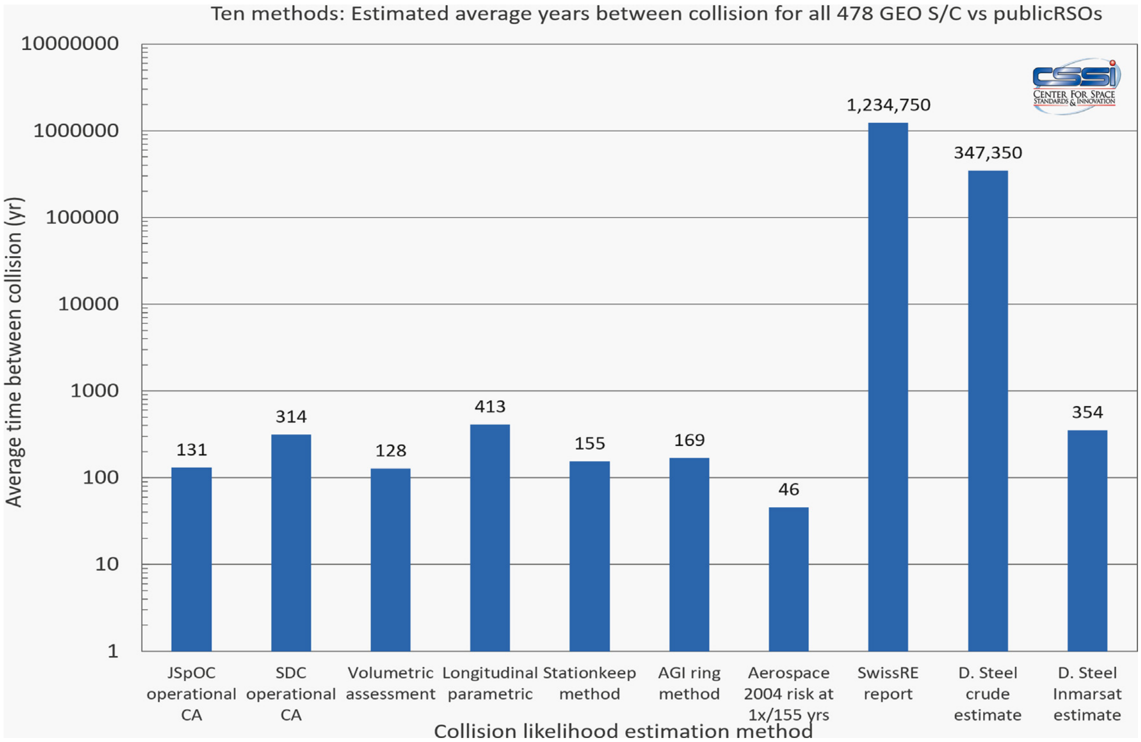

Fig. 62. Average years between collisions for 478 active GEO satellites versus the 2017 RSO public catalogue.

fragmentation), to hydrodynamic scenario (with little momentum transfer and extensive fragmentation)." This wide range of phenomena and resulting fragmentation types introduces a high degree of uncertainty in the resulting fragmentation field for a non-hypervelocity collision, with still greater uncertainty in imparted fragmentation velocity and direction.

14. The "dark horses" – highly-elliptical orbits and debris-on-debris

Despite the above comprehensive internal and external research findings and debris surveys, the results of this paper may still be missing some of the greatest GEO environment collision risks: conjunctions with currently untracked or poorly maintained HEOs. As stated in Ref. [63], "The space debris environment in the medium Earth orbit (MEO) region has not been systematically investigated so far and is thus largely unknown." HEOs are often "very difficult to observe optically around the

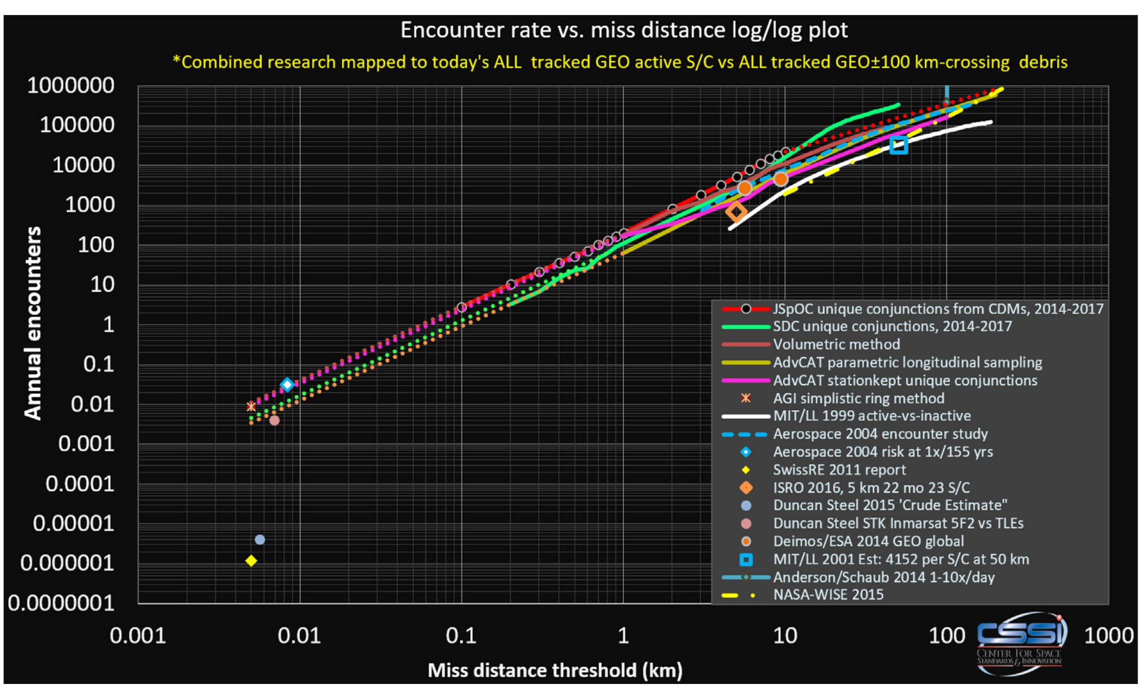

Fig. 63. Estimated GEO encounter rates for all active GEO satellites vs all tracked RSOs.

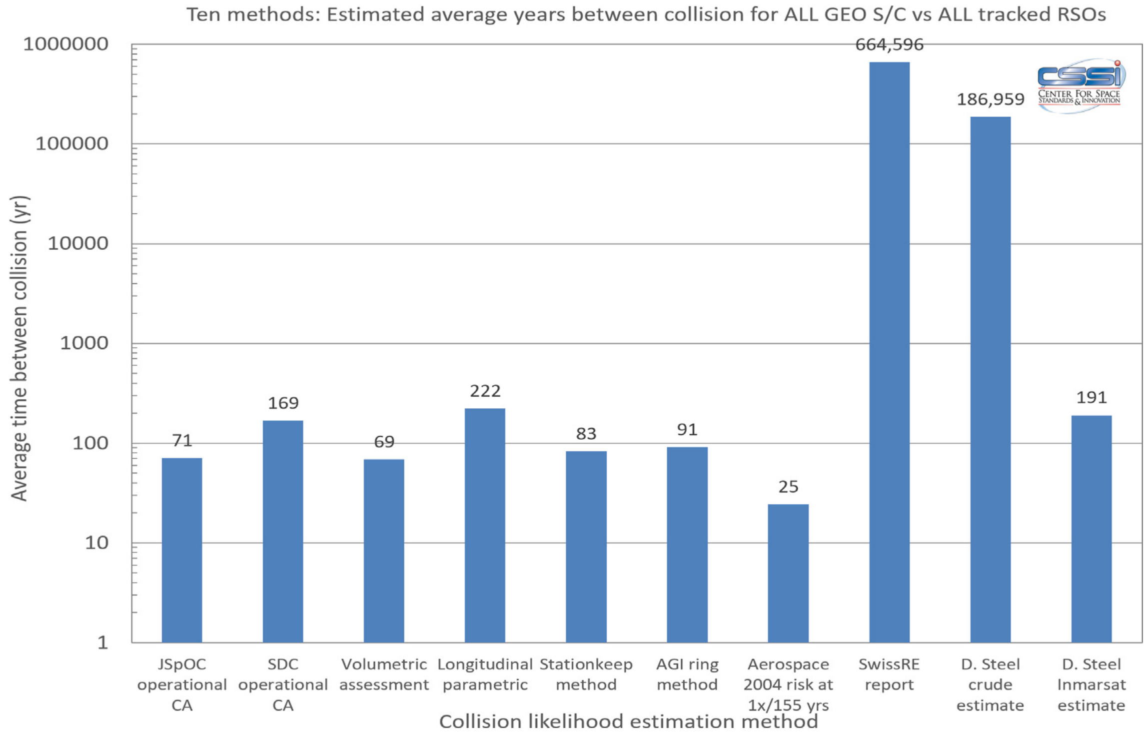

Fig. 64. Average years between collisions for all active GEO satellites vs all tracked RSOs.

perigee due to visibility constraints and the high angular velocities" [64]. Sensor coverage volumes are often ill-suited and not optimized for covering such a wide altitudinal variation that HEOs demand.

Some of these HEO debris fragments originated from HEO explosions. As stated in Ref. [65], "Since 2000, 42 out of the 90 non-deliberate, on-orbit explosions occurred in HEO, resulting on average in 26.9 observable objects across a large inclination range."

Unfortunately, we've also seen in Fig. 16 that such encounters exhibit the highest relative velocities (in excess of 3000 m/s) of all GEO conjunctions, thereby posing the greatest risk of doing environmental harm to the GEO belt.

A recent survey of HEOs [66] is consistent with [63] in that the survey indicates that "… there might well be a significant number of objects, possibly some population of debris, orbiting in Molniya-like orbits. An image of an inclined HEO object conjuncting crossing the GEO belt is shown in Fig. 70.

The other "dark horse" of GEO collision risk is debris-on-debris. Note that all of the assessments contained in this paper are based upon either (a) the currently-tracked RSO population, or (b) space population models that contain what we infer the current RSO population to be

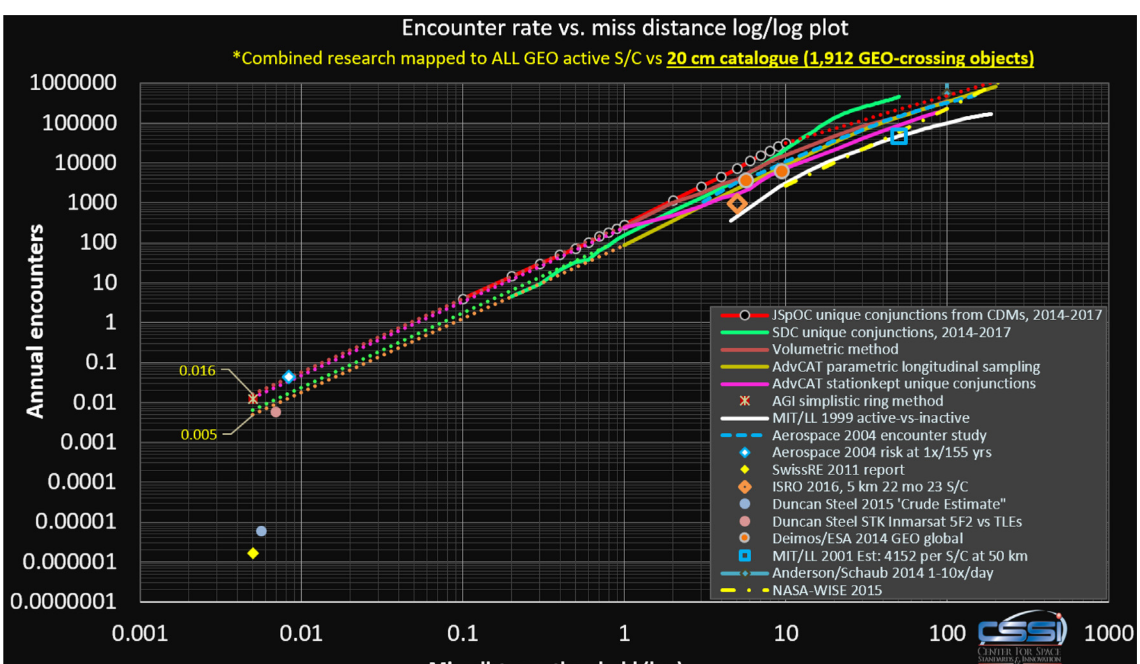

Fig. 65. Scaling of GEO encounter rates to all active GEO satellites vs 1912 estimated satellites and debris > 20 cm.

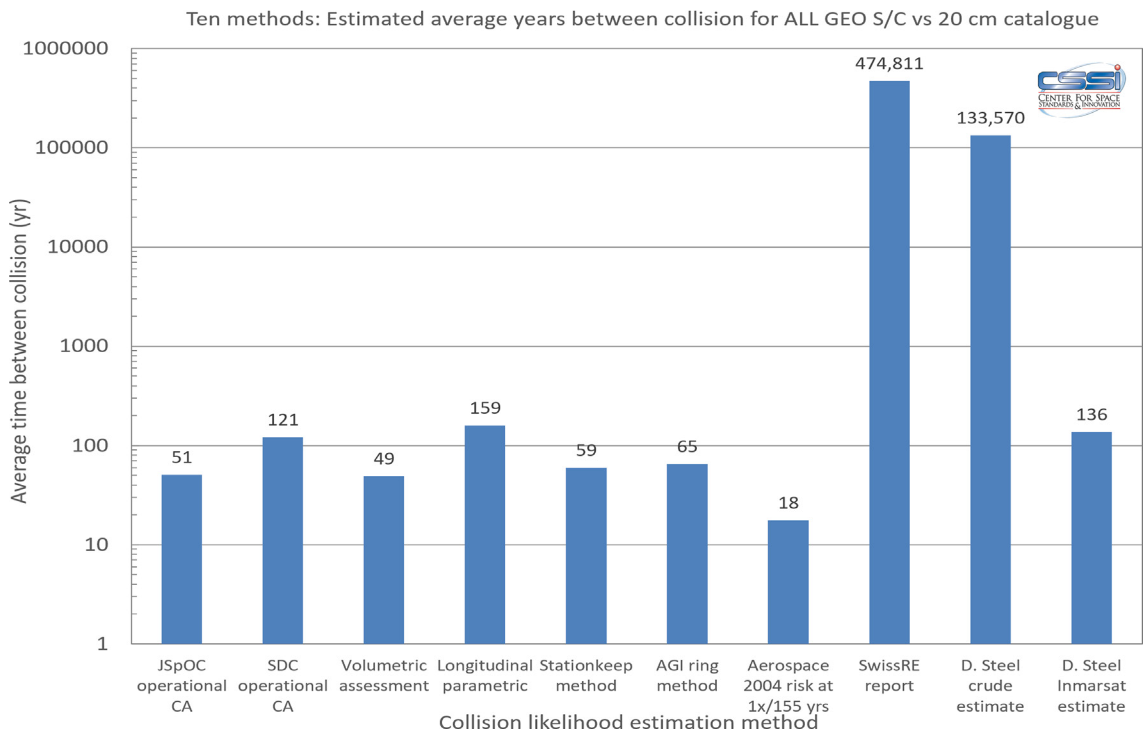

Fig. 66. Average years between collisions for all active GEO satellites vs 1912 estimated satellites and debris > 20 cm.

down to 1 cm object size. The moment that we have a significant collision in either GEO or the neighbouring GEO disposal orbit, these estimates will all change. McKnight [67] is conducting research into the risk of debris-on-debris collision for massive LEO objects. We advocate that the same be undertaken for the GEO belt to better understand the latent debris-on-debris risk.

15. Consequence of GEO collision

While the consequences of collision between two Boeing 702-class spacecraft are not fully known, it is fairly apparent that such an event could cause irreparable damage to the "prime real estate" known as the geosynchronous arc. Even for a "low" 800 m/s relative velocity (nearly 1800 miles per hour) collision of two satellites that are not designed to be materially robust in a collision, it's easy to envision a large debris field generated by such a collision event.

The Debris Risk Evolution and Dispersal (DREAD) tool [68,69] employs incorporated fragmentation event breakup models (including the NASA Standard Breakup Model) to determine the likelihood of post-collision (or explosion) fragments putting other space assets at risk as a

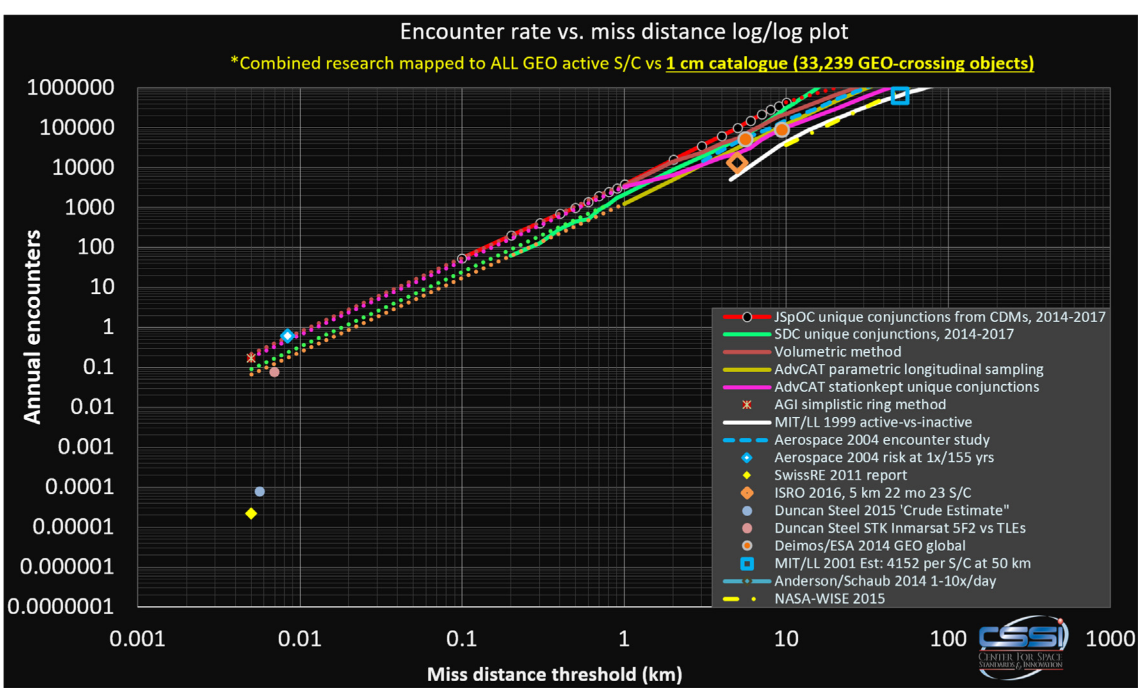

Fig. 67. Scaling of GEO encounter rates to all active GEO satellites vs 33,239 estimated satellites and debris > 1 cm.

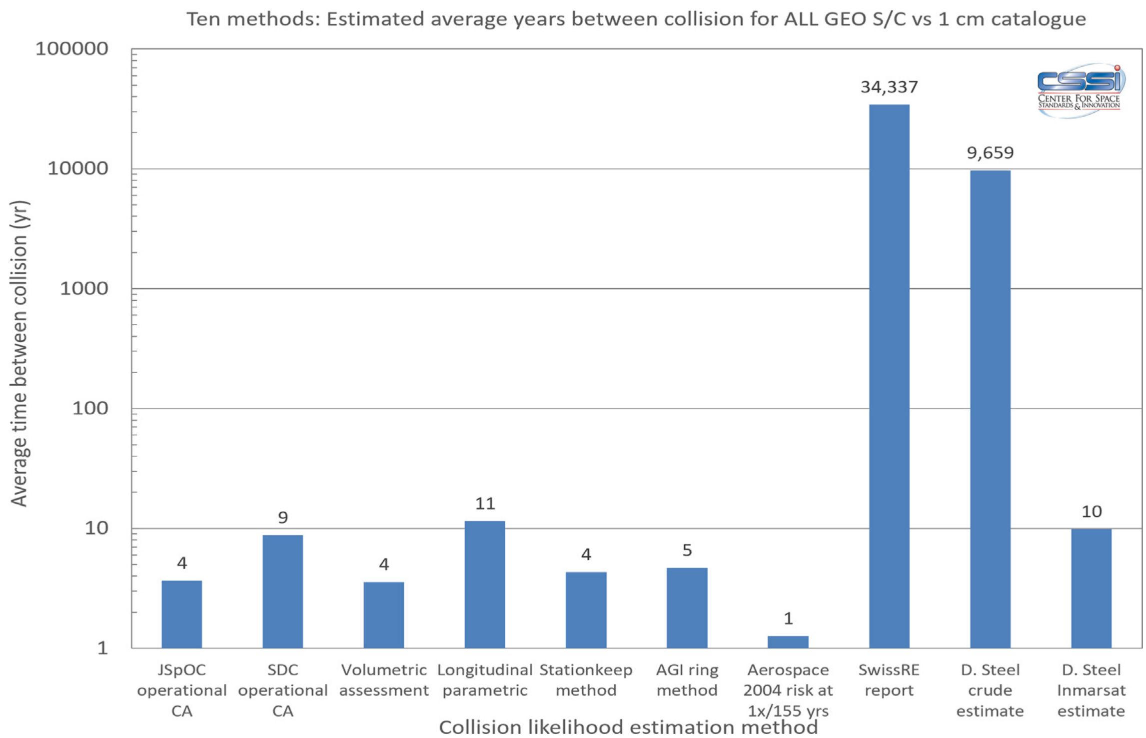

Fig. 68. Average years between collisions for all active GEO satellites vs 33,239 estimated satellites and debris > 1 cm.

function of time. The NASA Standard Breakup Model has been altered slightly to incorporate the sparse research [70] that has been done regarding non-hypervelocity fragmentation. Based upon that model, the result of a collision between a large active GEO satellite and a dead GEO satellite inclined at 15° could resemble that as shown in Fig. 71.

Aggregating this time-dispersing fragment risk cloud over a 28 h analysis timespan yields Fig. 72. Note how much of the GEO arc is placed at risk from this collision – a clear indication that all GEO satellite operators must use accurate, timely and actionable safety-of-flight data and procedures in order to protect and preserve the precious and financially lucrative GEO orbital arc.

Note that collision and encounter rates in graveyard orbits (> 235 km above GEO altitude) are also of concern because a high relative velocity collision (i.e. > 3 km/s) could also generate much GEO-crossing debris.

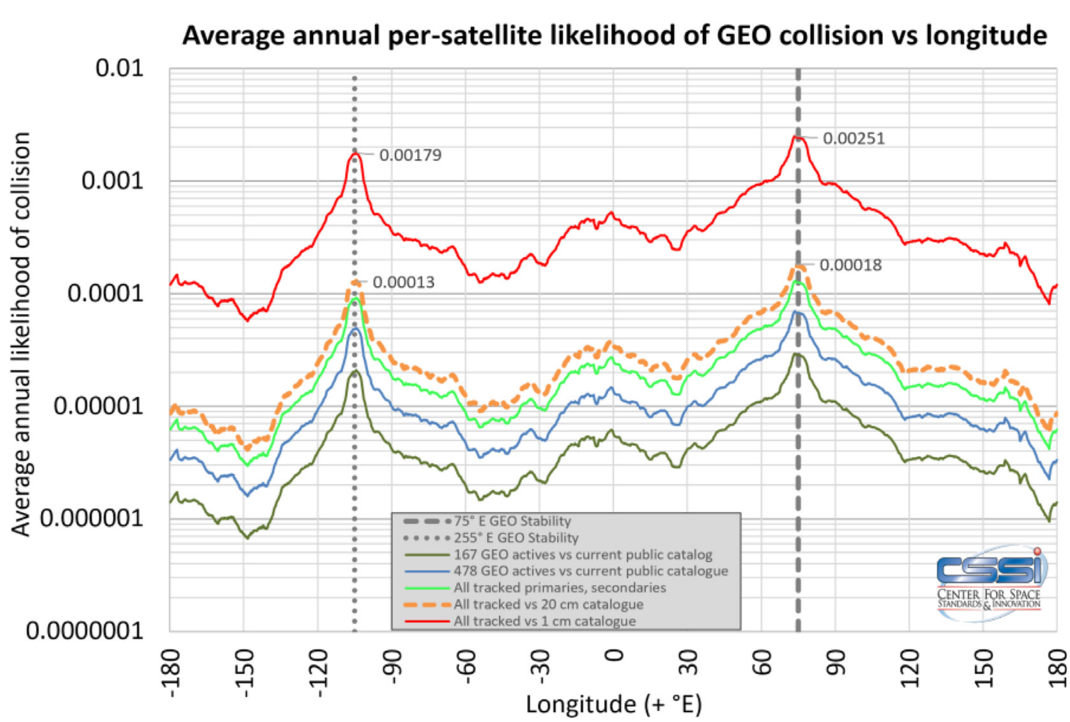

Fig. 69. Per-satellite likelihood of GEO collision by active/debris category and by longitude.

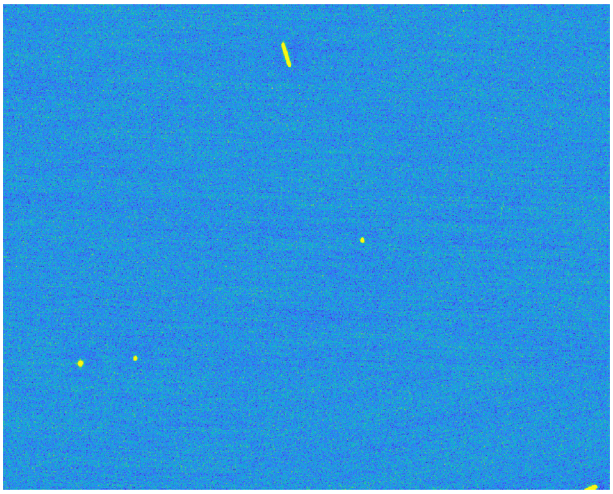

Fig. 70. HEO debris approaching GEO satellites [66] (included by permission of author).

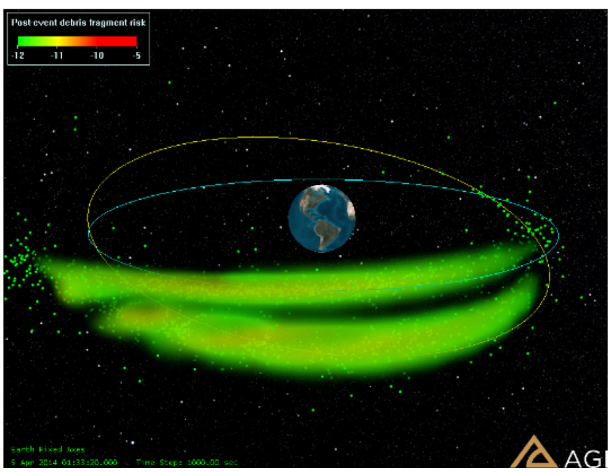

Fig. 71. Estimated fragmentation cloud dispersion volume at 15 h after collision (Earth-fixed frame).

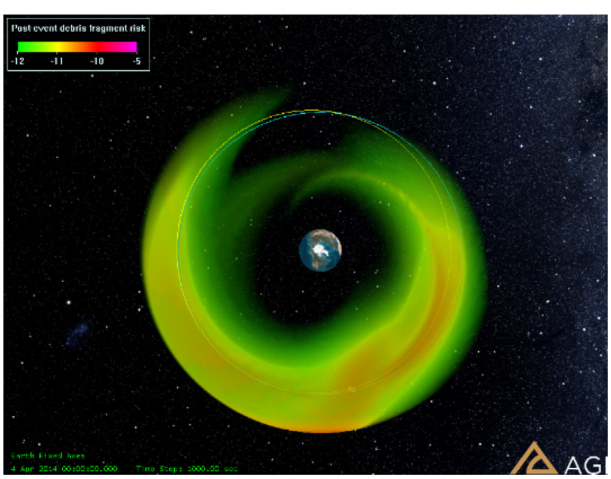

Fig. 72. Total fragmentation risk in the Earth-fixed frame, aggregated over a 28 h analysis timespan.

16. Potential path to effectively mitigate this GEO collision risk using SDC 2.0

The US Government maintains the only public catalogue of objects in space and makes it available through the Joint Space Operation Centre (JSpOC) in the form of Two Line Elements (TLE) and performs Conjunction Assessments (CA) for commercial operators. The current public Space catalogue today contains 16882 objects, 1300 of which are active LEO or GEO satellites.

CDM ID 8367303 Creation Date: 2017-03-28 15:58:13 UTC (1.7 hours ago) Upload Time: 2017-03-28 16:51:05 UTC (0.8 hours ago)		
Conjunction for 39215/ALPHASAT [+] and 10778/INTELSAT 4A-F6 [-]		
CDM min range at TCA (2017-04-01 08:11:28.589 UTC; 3.60 days out) = 0.900 km		
Ephemeris vs. CDM/TLE Comparison		
Primary	SP Range at TCA: 28.302 km	TLE Range at TCA: 21.679 km
Primary ephemeris epoch: 2017-03-23 00:00:00.000 UTC (5.74 days old)		
CDM vs. TLE Comparisons		
Primary Range at TCA: 49.916 km	Secondary Range at TCA: 1.550 km	
CDM Conjunction Comparisons		
SP vs. SP	TCA: 2017-04-01 08:11:28.589 UTC, 0.900 km	
Ephemeris vs. SP	**TCA: 2017-04-01 08:11:27.986 UTC, 28.575 km**	
Ephemeris vs. TLE	TCA: 2017-04-01 08:11:28.036 UTC, 28.320 km	
Ephemeris vs. Ephemeris	N/A	
Complete AGI Viewer Scenario		
Notes: • *Valid SDC ephemeris for primary* • *No SDC ephemeris available for secondary*		

Fig. 73. Ephemeris vs TLE/SP CA.

One of the limitations of the JSpOC model is that CA is performed using the Special Perturbations catalogue for both primary and secondary objects. While TLE and SP data can be sufficiently accurate for debris, JSpOC Batch Least Squares and their lack of manoeuvre modelling leads to large errors when fitting orbits to actively-manoeuvring satellites.

Inmarsat FD has observed differences in orbit of up to 30 km between O/O ephemeris and the TLE/SP catalogue.

Fig. 73 shows that the SP vs SP CA for Alphasat gives a 900 m minimum distance while the Ephemeris CA gives a minimum distance of 28.575 km vs the SP catalogue and 28.320 vs the TLE catalogue. Alphasat uses ionic propulsion with up to 2 burns a day and the Alphasat TLE and/or SP is not sufficiently accurate to rely on for collision avoidance purposes.

This limitation can be mitigated by sharing the orbital ephemeris including planned manoeuvres with the JSpOC. The conjunction assessment is then performed compared to the SP database and the ephemeris provided. However the ephemeris is used without the ability to combine or calibrate the operator ranging data with the JSpOC observations.

The Space Data Association (SDA) was formed in 2009 by the world's leading satellite operators with the mission to improve safety of flight via sharing of operational data and promotion of best practices across the industry. In partnership with its chosen technology provider, Analytical Graphics Inc. (AGI), the SDA developed the Space Data Center (SDC). SDC is a platform that ingests flight dynamics information from the member companies as well as other available sources of space object information to provide conjunction assessment and warning services.

From the previous sections it will have become clear that the collision likelihood at GEO is higher than has been publicized by the insurance industry, due to the vast amount of small, untracked objects, not included in publicly available catalogues.

The SDA recognises the need to improve current CA systems and together with AGI plans to deploy the SDC 2.0 system, which will alleviate gaps in three main areas:

1) Tracking smaller objects, down to 20 cm in size
2) The ability to fuse and calibrate operator ranging data with independent sensor data, removing delays and other biases
3) Warnings based on estimated actual probability of collision, using realistic covariance information, accurately predicted future orbital ephemerides and non-spherical hardbody shapes

The SDC 2.0 will use a fully independently generated debris and satellite catalogue of RSO down to 20 cm in size with system performance level requirements provided under a binding service level agreement with the SDA using multiple phenomenologies (optical and radar).

The system provides the ability to calibrate operator ranging data with independent sensor observations and combine the observations and ranging data to achieve the highest level of orbital accuracy.

More and more of today's GEO satellites are using electrical propulsion with 80 mN thrusters instead of a more conventional 10 N thruster normally used in a CPS scenario to give adequate separation. It used to be sufficient to perform a Collision Avoidance Manoeuvre 12 h prior a Conjunction Assessment, but with an electrical satellite, three days is needed.

Fundamental to an effective avoidance strategy is the need for every satellite operator to be warned in advance of an accurately-predicted conjunction likelihood or probability of collision, using realistic covariance data and an accurate prediction of the future orbital ephemerides, rather than relying on a distance threshold alone.

As executive members of the SDA, Inmarsat and SES believe the SDC 2.0 will provide more effective means of mitigating a predicted high risk conjunction and reducing the number of false alarms, keeping the space environment safe for current and future use.

17. Conclusions

Results indicate that a collision is likely to occur every 4 years for the entire GEO active satellite population against a 1 cm RSO catalogue, and every 50 years against a 20 cm RSO catalogue. This means that unless operators successfully mitigate this collision risk, the GEO orbital arc is and will remain at high risk of collision, with serious follow-on collision threat from post-fragmentation debris should a substantial GEO collision occur. Further, previous assertions that collision relative velocities are low (i.e., < 1 km/s) in GEO are disproven, with GEO relative velocities as high as 4 km/s identified.

Operators can address these grave concerns by deliberate pooling of best-of-breed SSA data to obtain timely and actionable conjunction warnings. The new SDC 2.0 embodies the concept that the best SSA data set is “ours” (i.e. the fusion of the best-available all-source SSA data). This includes aggregation of satellite operator and tracking networks' observations, orbit determination in a common framework using an advanced orbit determination approach, ingestion and propagation thru GEO satellite operator manoeuvre plans, and tracking and SSA on much smaller objects than are in the current JSpOC public RSO catalogue.

Six internal and 11 external independent techniques were used to assess this. The six internal GEO assessment techniques introduced in this paper offer new and comprehensive insights into GEO collision likelihood that are well-aligned with each other. Additionally, we characterized relative velocities, encounter angles and secondary RSO categories for three years of predicted GEO active satellite conjunctions.

We only found four prior estimates of GEO collision risk by other researchers, and the two [24,32] which were flux-based estimates were as much as four orders of magnitude lower then the other fifteen assessments (taken in aggregate) indicate. This disparity is clearly shown in Fig. 60, where most GEO collision likelihood and encounter rate estimates matched fairly well, allowing for expected variations introduced by longitudinal differences and the imperfect scaling and mapping methods we employed to “normalize” results to a common baseline.

Critically, we infer from this that simplistic flux-based GEO collision likelihood assessment methods fail to account for the synchronicity, high spatial variability and time-varying dynamics of this orbit regime, likely yielding erroneous results.

Acknowledgements

We gratefully acknowledge the contributions and cooperation of the US Air Force (both JSpOC and USSTRATCOM) in this research. Contributions by the ESA Space Debris Office are also greatly appreciated, as well as AGI's Jim Wilson and Jens Ramrath who extracted the Space Data Center conjunction results for our SDC analysis component. We also would like to thank Dr. Glenn Peterson of The Aerospace Corporation's Astrodynamics Department for his insights on this subject.

References

[1] Debris-control Report Card Cites Improvement by Geo Sat Owners, (15 August 2017) Space News http://spacenews.com/37861debris-control-report-card-cites-improvement-by-geo-sat-owners/.
[2] D.S. Portree, J.P. Loftus, Orbital Debris: a Chronology, (January 1999) NASA/TP-1999–208856.
[3] Space-track Website, (5 September 2017) www.space-track.org.
[4] CelesTrak SATCAT Boxscore, (5 September 2017) http://celestrak.com/satcat/boxscore.asp.
[5] CelesTrak Website, (27 August 2017) http://www.celestrak.com.
[6] S.K. Flegel, Multi-layer Insulation as Contribution to Orbital Debris, Dissertation Technischen Universität Carolo-Wilhelmina zu Braunschweig, 8 November 2013.
[7] H. Krag, H. Klinkrad, R. Jehn, S. Flegel, T. Schildknecht, Conclusions from ESA space debris telescope observations on space debris environment modelling, ESA Space Debris Conference, Darmstadt, Germany, 2009.
[8] D.S. McKnight, F.R. Di Pentino, New insights on the orbital debris collision hazard at GEO, Acta Astronaut. 85 (2013) 73–82 6 December 2012.
[9] T. Schildknecht, et al., Long-term evolution of high area-to-mass ratio objects in different orbital regions, 2012 AMOS Tech Conference, 11 September 2012.
[10] ESA Space Debris User Portal, (6 September 2017) https://sdup.esoc.esa.int/web/csdtf/home.
[11] D.L. Oltrogge, V. Braun, Using space population models to generate representative space object catalogues, AAS 2016 Space Flight Mechanics Conference, AAS 16–233, Napa CA, 16 February 2016.
[12] J. Murray-Krezan, S. Howard, P.D. Dao, D. Surka, GEO collision risk assessment based on analysis of NASA-WISE data and modeling, 16th Advanced Maui Optical and Space Surveillance Technologies (AMOS) Conference, September 15-18, 2015 (Maui, Hawai'i).
[13] D.L. Oltrogge, The commercial space operations center (ComSpOC), ITU Satellite Communication Symposium 2017, Bariloche, Argentina, 29–30 May 2017.
[14] D.L. Oltrogge, Current SSA realities and improved SSA & RFI mitigation via ComSpOC, SSA Panel, SpaceOps 2016 Conference, Daejeon, Korea, 18 May 2016.
[15] T. Schildknecht, et al., Long-term evolution of high area-to-mass ratio objects in different orbital regions, 2012 AMOS Tech Conference, 11 September 2012.
[16] Boeing Corporation, Boeing Satellites: Technical Specifications, (27 August 2017) http://www.boeing.com/space/boeing-satellite-family/.
[17] Space Daily, Hughes Monitors Solar Array Deployment, (21 February 2000) http://www.spacedaily.com/news/panamsat-00d.html.
[18] P.V. Anderson, H. Schaub, Methodology for characterizing high-risk orbital debris in the geosynchronous orbit regime, Adv. Space Res. 57 (2016) 604–619.
[19] ISBN 1-884989-17-9, Applied Orbit Perturbation and Maintenance, The Aerospace Corporation Press, 2005, p. 63 Chao.
[20] A.N. Nazarenko, Modeling Space Debris, Institute of Space Studies, 2013 ISBN 978-5-9903101-6-2.
[21] Handbook of Geostationary Orbits, Springer Science + Business Media, Dordrecht, 1994, p. 90 vol. 3. ISBN 978-90-481-4453-2.
[22] B.W. Hansen, M.E. Sorge, Summarizing the general effects of breakup debris in GEO, AAS 13-844, 2013.
[23] S.K. Flegel, Towards state uncertainty accuracy requirements for actionable GEO collision risk assessments, IAC-17,A6,2,3,x39941, International Astronautical Congress 2017, Adelaide, Australia, 26 September 2017.
[24] SwissRe insurance company, Space Debris: on Collision Course for Insurers? (2011) http://media.swissre.com/documents/Publ11_Space + debris.pdf.
[25] S. Frey, et al., Impact of end-of-life manoeuvres on the resident populations in protected regions, IAC–16–A6.4.1, 67th International Astronautical Congress, Guadalajara, Mexico, 26-30 September, 2016.
[26] L. Vance, The Value of Orbital Debris removal, Raytheon Company, 10 November 2010.
[27] R.A. LeClair, Probability of Collision in the Geostationary Orbit, MIT Lincoln Laboratory, 2001.
[28] R.A. LeClair, R. Sridharan, Probability of collision in the geostationary orbit, ESA Space Debris Conference, Darmstadt, Germany, 2001.
[29] W.H. Ailor, G.E. Peterson, Collision avoidance as a debris mitigation measure, IAC-04-IAA.5.12.3.01, International Astronautical Congress 2004, Vancouver, B.C., Canada, 4–8 October 2004.
[30] P.V. Anderson, H. Schaub, Longitude-dependent effects of fragmentation events in the geosynchronous orbit regime, AAS 14-321, AAS/AIAA Space Flight Mechanics Meeting, Sante Fe, New Mexico USA, 26–30 January 2014.
[31] G. Peterson, Determining object sizes from radar cross section for collision avoidance, AAS 05-307, 2005.

[32] D. Steel, The orbital debris collision hazard for satellites in geostationary orbit, http://www.duncansteel.com/archives/1475, (29 April 2015).
[33] H.P. Singh, List of satellites launched by ISRO, http://www.jagranjosh.com/general-knowledge/list-of-satellites-launched-by-isro-1454322647-1, (1 February 2016).
[34] M.R.R. Kannan, P.E. Manikantan, D. Kumar, S.K. Vasanth, S. Selvamani, K. Guruprasad, R. Jantikar, B.N. Rao, A. Narayana, H.P. Shenoy, Collision avoidance assessment and mitigation measures for controlled GEO/GSO spacecraft with orbital debris, 7th European Conference on Space Debris, ESA/ESOC, Darmstadt/Germany, 18–21 April 2017.
[35] N. Sanchez-Ortiz, R. Domınguez-Gonzalez, H. Krag, Evaluation of minimum coverage size and orbital accuracy at different orbital regimes for one order of magnitude reduction of the catastrophic collision risk, Adv. Space Res. 55 (2015) 1673–1686.
[36] P.V. Anderson, H. Schaub, Longitude-dependent effects of fragmentation events in the geosynchronous orbit regime, Acta Astronaut. 105 (2014) 285–297 16 September 2014.
[37] Sal Alfano, Dan Oltrogge, Volumetric assessment of encounter probability, AIAA/AAS Astrodynamics Specialist Conference, San Diego, CA, 8 August 2014.
[38] S. Alfano, D.L. Oltrogge, Volumetric encounter analysis enhancements, Paper No. AAS 15–581, AAS/AIAA Astrodynamics Specialist Conference, Vail, CO, 10-13 August, 2015.
[39] D.L. Oltrogge, S. Alfano, Collision risk in low Earth orbit, 2016 International Astronautical Congress, Guadalajara, Mexico, 23 September 2016.
[40] G.E. Peterson, Comparison of collision risk from COLA and kinetic gas theory for sun-synchronous orbits, AAS-05-123, AAS/AIAA Space Flight Mechanics Meeting, Copper Mountain, Colorado USA, 23–27 January 2005.
[41] H.B. Dwight, Tables of Integrals and Other Mathematical Data, fourth ed., The Macmillan Company, 1961, p. 132.
[42] HyperPhysics, Georgia State University, 6 September 2017, http://hyperphysics.phy-astr.gsu.edu/hbase/Kinetic/menfre.html.
[43] P.V. Anderson, H. Schaub, Local debris congestion in the geosynchronous environment with population augmentation, Acta Astro. 94 (2014) 619–628 21 August 2013.
[44] D.L. Oltrogge, T.S. Kelso, Getting to know our space population from the public catalogue, Paper AAS 11-416, Girdwood AK, 1 August 2011.
[45] Brendan Houlton, Dan Oltrogge, Commercial space operations center (ComSpOC): a commercial alternative for space situational awareness (SSA), 30th Space Symposium, Technical Track, Colorado Springs, CO, 21 May 2014.
[46] D.L. Oltrogge, ComSpOC update and operational benefits, 31st Space Symposium, Colorado Springs, CO, 13–14 Apr 2015.
[47] T.J. Johnson, Commercial SSA, 40th AAS GN&C Conference, Breckenridge, CO, 6 February 2017.
[48] D.L. Oltrogge, The commercial space operations center (ComSpOC), ITU Satellite Communication Symposium, 2017 29–30 May 2017, Bariloche, Argentina.
[49] Space Data Association, (13 September 2017) http://www.space-data.org/sda/.
[50] P.V. Anderson, H. Schaub, Local orbital debris flux study in the geostationary ring, Adv. Space Res. 51 (2013) 2195–2206.
[51] F.R. Hoots, P.W. Schumacher, R.A. Glover, History of analytical orbit modeling in the U.S. Space surveillance system, J. Guid. Contr. Dynam. 27 (2) (March-April 2004).
[52] GOES 13 weather satellite returns to service after hit from micrometeoroid, Satellite Today, 12 June 2013. http://www.satellitetoday.com/publications/st/curated/2013/06/12/goes-13-weather-satellite-returns-to-service-after-hit-from-micrometeoroid/, .
[53] NOAA GOES-13 incident report per Work, K., NOAA Flight Ops Team, (14 September 2017).
[54] Meteosat-8 Failure, (13 September 2017) http://sat-nd.com/failures/msg1.html.
[55] Russian Telecom Satellite Fails after Sudden Impact, (30 March 2006) Space Daily http://www.spacedaily.com/reports/Russian_Telecom_Satellite_Fails_After_Sudden_Impact.html.
[56] Space Debris Incidents Involving Soviet/Russian Launches, (14 September 2017) Observing Systems Capability Analysis and Review (OSCAR) Tool https://www.wmo-sat.info/oscar/satellites/view/149%20SPACE%20DEBRIS%20INCIDENTS%20INVOLVING%20SOVIET/RUSSIAN%20LAUNCHES.
[57] NASA Technical Memorandum NASA/TM-2008-214779, History of On-orbit Satellite Fragmentations, fourteenth ed., NASA Orbital Debris Program Office, June 2008.
[58] J. Gabbard, History of Satellite Breakups in Space, NORAD Headquarters, 1 July 1982.
[59] Satellite News Digest, Satellite Outages and Failures, (14 September 2017) http://sat-nd.com/failures/.
[60] Gunter's Space Page, Ekspress-am 11, (14 September 2017) http://space.skyrocket.de/doc_sdat/ekspress-am-11.htm.
[61] N.L. Johnson, et al., NASA's new breakup model of evolve 4.0, Adv. Space Res. 28 (9) (2001) 1377–1384.
[62] D. McKnight, Low Velocity Collisions in GEO, (2015).
[63] J. Silha, T. Schildknecht, A. Hinze, T. Flohrer, A. Vananti, An optical survey for space debris on highly eccentric and inclined MEO orbits, Adv. Space Res. 59 (Jan. 2017) 181–192.
[64] A. Hinze, T. Schildknecht, T. Flohrer, H. Krag, Results of space debris survey observations on highly-eccentric MEO orbits, Presented at the 6th European Conference on Space Debris, vol. 723, 2013, p. 140.
[65] S. Frey, C. Colombo, S. Lemmens, H. Krag, Evolution of fragmentation cloud in highly eccentric orbit using representative objects, IAC 2017, IAC-17–A6.2.6, International Astronautical Congress 2017, Adelaide, Australia, 24 September 2017.
[66] J.T. McGraw, P.C. Zimmer, M.R. Ackermann, Ever wonder What's in Molniya? We do, AMOS SSA Conference, Maui, Hawai'i, 20 September 2017.
[67] D. McKnight, et al., Preliminary analysis of two years of the massive collision monitoring activity, IAC-17,A6,2,1,x35961, 2017 International Astronautical Congress, Adelaide, Australia, 26 September 2017.
[68] D.A. Vallado, D.L. Oltrogge, “Fragmentation event debris field evolution using 3d volumetric risk assessment, ESA Space Debris Conference, ESDC-17-738, Darmstadt, Germany, 24 April 2017.
[69] D.L. Oltrogge, D.A. Vallado, Application of new debris risk evolution and dissipation (dread) tool to characterize post-fragmentation risk, 2017 Astrodynamics Specialist Conference, Stevenson WA, AAS 17-600, 22 August 2017.
[70] Toshiya Hanada, Developing a low-velocity collision model based on the NASA standard breakup model, Space Debris 2 (4) (2000) 233–247.